

# ARRAY SEISMOLOGY: METHODS AND APPLICATIONS

Sebastian Rost<sup>1</sup>

Department of Earth Sciences  
University of California  
Santa Cruz, California, USA

Christine Thomas<sup>2</sup>

Department of Earth Sciences  
University of Liverpool  
Liverpool, UK

Received 16 March 2001; revised 22 May 2002; accepted 9 September 2002; published 5 December 2002.

[1] Since their development in the 1960s, seismic arrays have given a new impulse to seismology. Recordings from many uniform seismometers in a well-defined, closely spaced configuration produce high-quality and homogeneous data sets, which can be used to study the Earth's structure in great detail. Apart from an improvement of the signal-to-noise ratio due to the simple summation of the individual array recordings, seismological arrays can be used in many different ways to study the fine-scale structure of the Earth's interior. They have helped to study such different structures as the interior of volcanos, continental crust and lithosphere, global variations of seismic velocities in the mantle, the core-mantle boundary and the structure of the inner core. For this purpose many different, specialized array techniques have been developed and applied to an increasing number of high-quality array data sets. Most array methods use the ability of seismic arrays to measure the vector velocity of an incident wave front, i.e., slowness and back azimuth. This information can be used to distinguish between different seismic phases, separate waves from different seismic events and improve the signal-to-noise ratio by stacking with respect to the varying slowness of different phases. The vector velocity information of scattered or reflected phases can be used to determine the region of the Earth from whence the seismic energy comes and with what structures it inter-

acted. Therefore seismic arrays are perfectly suited to study the small-scale structure and variations of the material properties of the Earth. In this review we will give an introduction to various array techniques which have been developed since the 1960s. For each of these array techniques we give the basic mathematical equations and show examples of applications. The advantages and disadvantages and the appropriate applications and restrictions of the techniques will also be discussed. The main methods discussed are the beam-forming method, which forms the basis for several other methods, different slant stacking techniques, and frequency-wave number analysis. Finally, some methods used in exploration geophysics that have been adopted for global seismology are introduced. This is followed by a description of temporary and permanent arrays installed in the past, as well as existing arrays and seismic networks. We highlight their purposes and discuss briefly the advantages and disadvantages of different array configurations.

**INDEX TERMS:** 7294 Seismology: Instruments and techniques; 1734 History of Geophysics: Seismology; 1794 History of Geophysics: Instruments and techniques; **KEYWORDS:** array seismology; array methods; geophysics; earthquake and nuclear explosion seismology

**Citation:** Rost, S., and C. Thomas, Array seismology: Methods and applications, *Rev. Geophys.*, 40(3), 1008, doi:10.1029/2000RG000100, 2002.

## 1. INTRODUCTION

[2] Since the beginning of the 1960s a new type of seismological tool helped to lower the detection threshold of global earthquakes and nuclear explosions and provided a possibility of resolving the fine structure of the Earth's interior [e.g., Birtill and Whiteway, 1965; Whiteway, 1966; Wright, 1972; Doornbos and Husebye, 1972; Weber *et al.*, 1996; Kværna, 1989]. These seismological instruments consist of numerous seismometers placed at discrete points in a well-defined configuration and are called seismological arrays [Husebye and Ruud,

1989]. Seismic arrays were originally built to detect and identify nuclear explosions and have been used for such ever since. They are closely related to studies of the seismic source, especially to discriminate between nuclear explosions and (natural) earthquakes, and they have lowered the global detection threshold of underground nuclear explosions to yields as low as 1 kt and below [Douglas *et al.*, 1999; Douglas, 2002]. By offering seismologists dense spatial samples of the seismic wavefield at various sites on the Earth's surface, seismic arrays led to refined velocity models of the Earth's interior [e.g. Káráson and van der Hilst, 2001], high-resolution tomographic images on regional scales [e.g., Arlitt *et al.*, 1999; Ritter *et al.*, 2001], and detection of small-scale structures in the Earth's mantle [e.g., Castle and Creager, 1999; Krüger *et al.*, 2001] and at the core-

<sup>1</sup>Formerly at Institut für Geophysik, Universität Göttingen, Göttingen, Germany.

<sup>2</sup>Formerly at Department of Earth Science, University of Leeds, Leeds, UK.

mantle boundary [e.g., *Thomas et al.*, 1999; *Rost and Revenaugh*, 2001] and of heterogeneities in the inner core [e.g., *Vidale and Earle*, 2000] to name but a few benefits.

[3] Seismic array analysis can be described by the same basic mathematical principles as those that apply for arrays of antennae used in radioastronomy or radar science [*Harjes and Henger*, 1973], and they have the same effect on seismology as the widespread use of powerful telescopes has on modern astronomy. One of the main advantages of seismic arrays, compared to single seismological stations, is the improvement of the signal-to-noise ratio (SNR) due to the summation of the individual recordings of the array stations. In addition, the seismic arrays can determine directional information of seismic signals; that is, it is possible to locate the source of a seismic signal by a single array measurement. Numerous techniques to perform this task have been developed. This review will introduce only some of these. For additional detail, see earlier works by, for example, *Aki and Richards* [1980], *Kanasewich* [1981], *Haykin* [1985], and *Ingate et al.* [1985].

[4] In the first part of this review we introduce the main processing techniques used with seismological arrays. We give the basic mathematical formalism as well as examples of applications of the method, and we discuss advantages and restrictions of the methods. In section 3 we introduce both historical and more recently developed methods. Subsequently, we give an overview of installed seismological arrays. Starting with a historical overview on early arrays, we discuss the different existing types of arrays and their main use. At the end of this overview we give suggestions on the configuration for future arrays especially suited to study Earth's deep interior, and we conclude the review with a discussion on the advantages and disadvantages of array seismology.

## 2. WHY SHOULD WE USE ARRAYS?

[5] Seismic arrays are expensive to deploy and to maintain. So what are the advantages of arrays over single stations for global seismology?

[6] Through the use of array data and the appropriate processing techniques the relative size of seismic signals, with respect to the ambient seismic noise within the Earth, is increased. This enables us to study phases that normally do not show up in seismograms of single stations with amplitudes large enough to study travel times and/or waveforms. This is the primary reason why seismic arrays prove very useful in studies of the small-scale structure of the Earth's interior, in source mechanism studies and in forensic seismology.

[7] Besides the large-scale images of Earth structure derived from global tomography that are only possible to produce with global networks, many regional tomographic studies have been made possible with seismic arrays [e.g., *Achauer and the KRISP Working Group*, 1994; *Ritter et al.*, 1998, 2001]. Arrays helped to resolve

fine-scale structure well below the resolution level of global seismology in many different places in the Earth, from the crust using body waves [e.g., *Rothert and Ritter*, 2001] and surface waves [e.g., *Pavlis and Mahdi*, 1996; *Cotte et al.*, 2000], the upper mantle [e.g., *Rost and Weber*, 2001], the lower mantle [e.g., *Castle and Creager*, 1999; *Krüger et al.*, 2001], the core-mantle boundary [e.g., *Kanasewich et al.*, 1973b; *Wysession et al.*, 1999; *Thomas et al.*, 1999; *Rost and Revenaugh*, 2001], and the inner core [e.g., *Vidale et al.*, 2000; *Vidale and Earle*, 2000; *Helffrich et al.*, 2002]. A different branch of seismology that benefited from arrays is “forensic seismology” [*Koper et al.*, 2001]. In our opinion, array seismology has the potential to refine the scale at which Earth's interior is resolved, and we think that with the deployment of more temporary and permanent arrays more questions about how the Earth works will be answered, and perhaps many more will be raised.

## 3. METHODS

[8] Most array methods assume a plane wave arriving at the array. This is a good approximation for wave fronts from teleseismic events but is a restriction for the study of near-receiver structures. The propagation direction of elastic waves traveling in a spherical Earth and arriving at a seismological array can be described by two parameters (Figure 1):

a) (1) vertical incident angle  $i$  and (2) back azimuth  $\theta$ . In practice, not the incident angle  $i$  but the inverse of the apparent velocity of the wave front across the array  $1/v_{\text{app}}$  is used. This parameter is called slowness  $u$ :

$$u = \frac{1}{v_{\text{app}}} = \frac{\sin i}{v_0}, \quad (1)$$

with  $v_0$  as the medium velocity beneath the array.

b) back azimuth  $\theta$  is the angle of the wave front arriving at the array measured between north and the direction to the epicenter in degrees.

[9] Both parameters are combined in the slowness vector  $\mathbf{u}$ . In a spherical geometry this is

$$\begin{aligned} \mathbf{u} &= (u_x, u_y, u_z) \\ &= \left( \frac{\sin \theta}{v_{\text{app}}}, \frac{\cos \theta}{v_{\text{app}}}, \frac{1}{v_{\text{app}} \tan i} \right) \\ &= u_{\text{hor}} \left( \sin \theta, \cos \theta, \frac{1}{\tan i} \right) \\ &= \frac{1}{v_0} (\sin i \sin \theta, \sin i \cos \theta, \cos i). \end{aligned} \quad (2)$$

The geometry of the slowness vector is shown in Figure 2. The slowness vector  $\mathbf{u}$  points into the direction of wave propagation, and its modulus is the reciprocal of

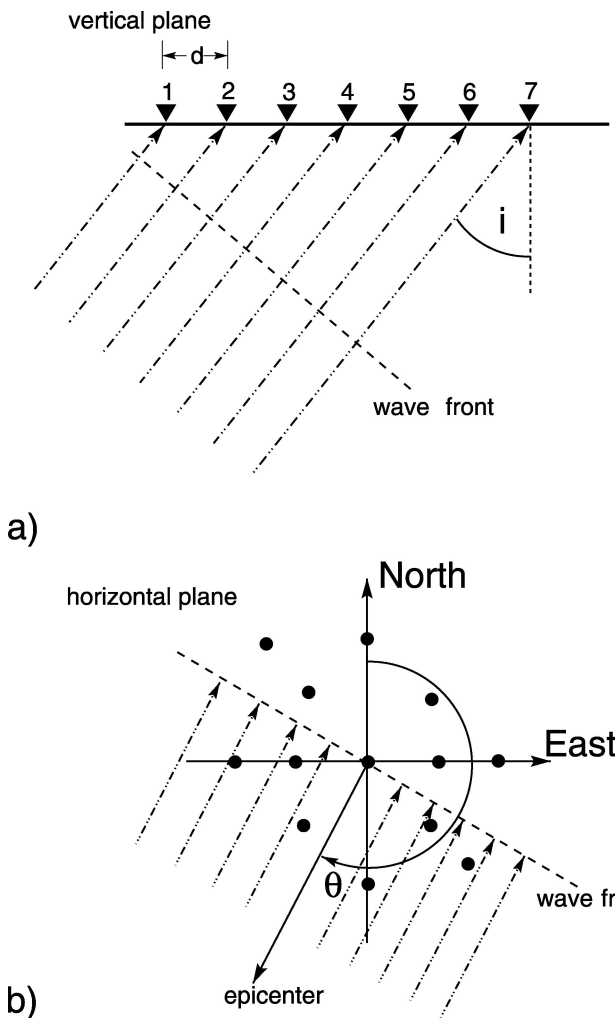


**Figure 1.** (a) The vertical plane of an incident wave front crossing an array at an angle of incidence  $i$ . (b) Sketch of the horizontal plane of an incident plane wave arriving with a back azimuth  $\theta$ .

the wave speed. The ray parameter  $p$  and the horizontal slowness  $u_{\text{hor}}$  are interdependent:

$$p = \frac{r \sin i}{v} = \frac{R_0 \sin i}{v_0} = R_0 u_{\text{hor}}. \quad (3)$$

$R_0$  is the distance of the turning point of the ray from the Earth's center. Therefore the velocity at the turning point of the ray can be determined from the slowness. More importantly, the slowness is a way to identify different phases traveling through the Earth's interior as it is unique to a given phase in a one-dimensional Earth.

[10] In the following we will introduce basic array methods widely used in global seismology. Many more methods developed for special purposes exist, and we refer the reader to the specific literature.

### 3.1. Beam Forming

[11] An important use of seismic arrays is the separation of coherent signals and noise. The basic method to

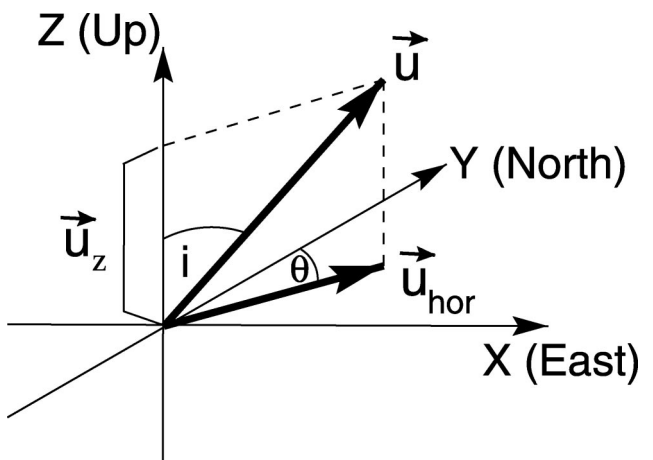


**Figure 2.** Components of the slowness vector  $\mathbf{u}$ . The components incident angle  $i$  and back azimuth  $\theta$  (compare Figure 1) are marked. The slowness vector is normal to the incident wave front.

separate coherent and incoherent parts of the recorded signal is array beam forming.

[12] Beam forming uses the differential travel times of the plane wave front due to a specific slowness and back azimuth to individual array stations. If the single-station recordings are appropriately shifted in time for a certain back azimuth and slowness, all signals with the matching back azimuth and slowness will sum constructively.

[13] The individual stations in an array are positioned at the location  $\mathbf{r}_j$  (Figure 3). The absolute value  $r = |\mathbf{r}_j|$  describes the distance of the instrument  $j$  in all three directions from the array center. The array center is either a central instrument or the geometrical center of the array. The incident wave field with the signal  $f(t)$  and noise  $n_i(t)$  with variance  $\sigma^2$  is recorded at the center station of the array as the time series:

$$x_{\text{center}}(t) = f(t) + n_i(t). \quad (4)$$

Owing to the different locations of the array stations the incident wave front has different travel times to each station. The travel time difference is dependent on the slowness of the wave front and the sensor location.

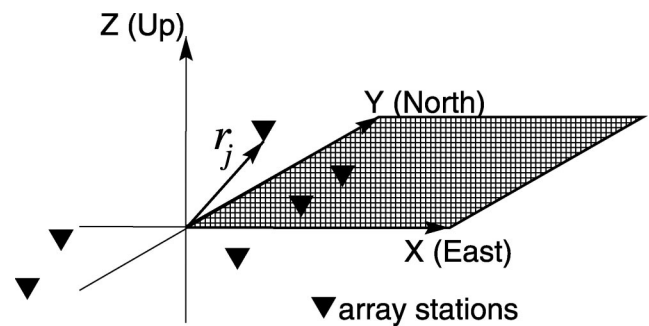


**Figure 3.** The definition of the sensor position vectors  $\mathbf{r}_j$ . The center of the array is assumed to be in the center of the Cartesian coordinate system.

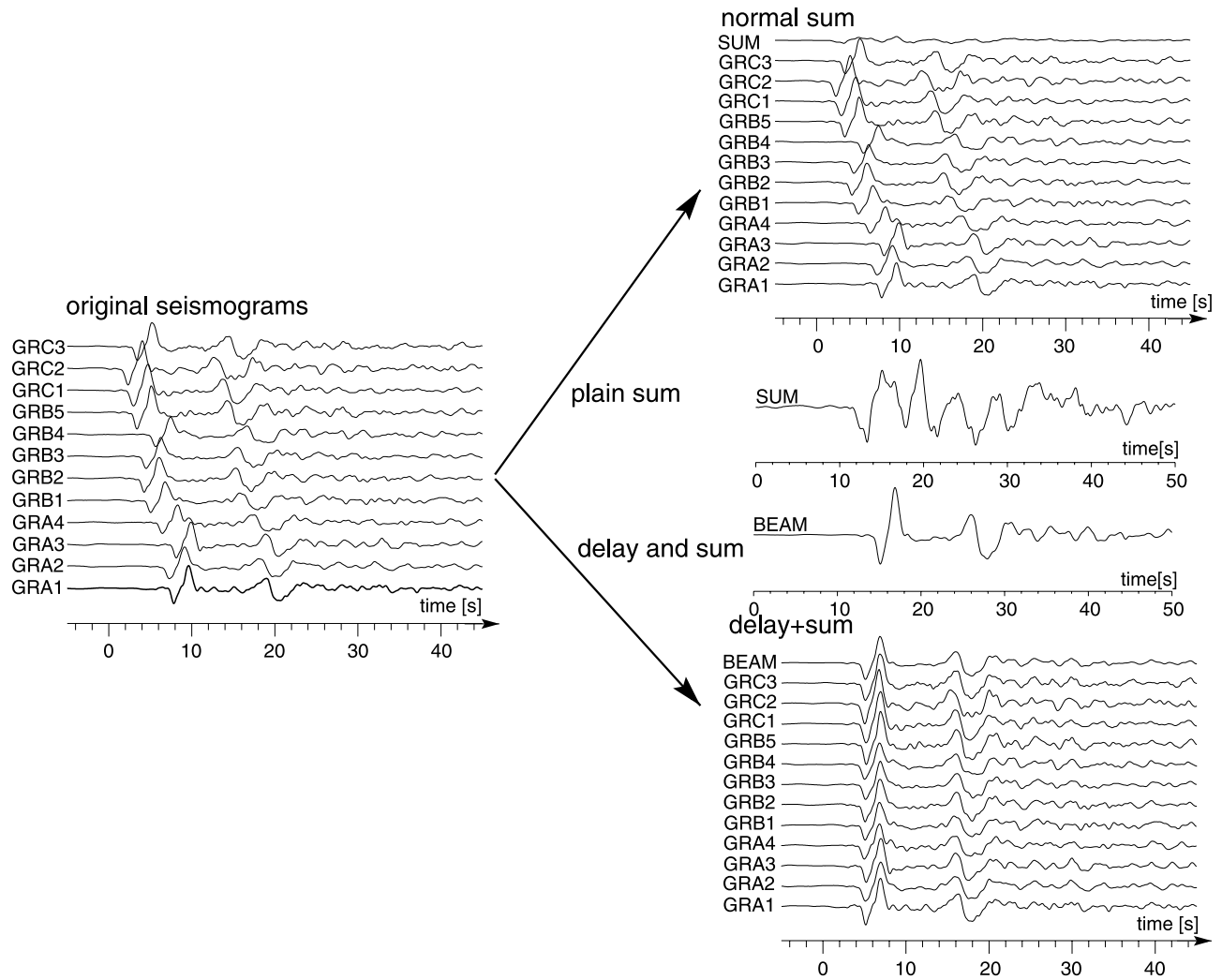


**Figure 4.** Example of the plain sum and “delay and sum” method for an event in the Lake Tanganyika region (Tanzania/Burundi) (2 October 2000 at 0225 UT, depth of 34 km,  $M_b = 6.1$ ,  $\Delta = 59.9^\circ$ , and  $\theta = 157.35^\circ$ ) recorded at the Gräfenberg array (GRF) (GRA1 to GRC3). The left-hand side shows the traces as recorded by the array stations. The right-hand plots show the results of (top) a plain sum and (bottom) a delay and sum. High amplitudes and no signal distortion is achieved by the delay and sum method.

Therefore station  $i$  with the location  $\mathbf{r}_i$  records the time series:

$$x_i(t) = f(t - \mathbf{r}_i \cdot \mathbf{u}_{\text{hor}}) + n_i(t) \quad (5)$$

with  $\mathbf{r}_i$  representing the location vector of station  $i$  and  $\mathbf{u}_{\text{hor}}$  representing the horizontal slowness vector. A trace, where the time shift is removed, can be calculated by

$$\tilde{x}_i(t) = x_i(t + \mathbf{r}_i \cdot \mathbf{u}_{\text{hor}}) = f(t) + n_i(t + \mathbf{r}_i \cdot \mathbf{u}_{\text{hor}}). \quad (6)$$

The “delay and sum” beam trace for an array with  $M$  components is then computed by

$$b(t) = \frac{1}{M} \sum_{i=1}^M \tilde{x}_i(t) = f(t) + \frac{1}{M} \sum_{i=1}^M n_i(t + \mathbf{r}_i \cdot \mathbf{u}_{\text{hor}}). \quad (7)$$

The beam forming method amplifies phases with the appropriate slowness, while suppressing incoherent noise and phases with different slowness. Using beam

forming, seismic arrays act as a wave number filter. More elaborate wave number filter methods have been developed for array seismology [Douglas, 1998]. The noise suppression is dependent on the number of stations used for the processing. A good approximation [Harjes and Henger, 1973] of the improvement of the signal-to-noise ratio (SNR) of the array  $S$  in comparison with the SNR of the single array station  $s$  is

$$S \approx \sqrt{M} s \quad (8)$$

for an array with  $M$  components, assuming perfectly coherent signals  $f(t)$  at every array station, and completely uncorrelated noise  $n_i(t)$ .

[14] An example of the advantage of the beam forming method is shown in Figure 4. Shown are recordings of the Gräfenberg array (GRF) of an event in the Lake Tanganyika region (Tanzania/Burundi). The left-hand side shows the traces as recorded at

GRF. A plain summation of the traces leads to a small-amplitude sum trace with distorted waveforms (right top panel), while a summation after shifting the trace for the slowness aligns the wavelet and leads to a clear high-amplitude waveform in the summation trace (right bottom panel).

[15] The beam-forming method works only for a discrete slowness and back azimuth combination. Therefore the complete slowness vector of a phase must be known for successful beam forming. Incorrect values of slowness and back azimuth result in lower signal amplitudes and signal distortion. Even if the theoretical slowness and back azimuth are known, several parameters, for example, local variation of wave speeds beneath the array stations [Berteussen, 1976; Krüger and Weber, 1992], can cause slowness and back azimuth deviations from theoretical values. If the structure beneath the array is well known, these parameters can be taken into account by mislocation vectors. In addition, for a successful stack of the waveforms across the array the waveforms must be similar, i.e., coherent. This makes the use of beam forming methods difficult for networks with nonuniform station equipment and for large-aperture arrays.

### 3.2. Vespa Process–Slant Stacks

[16] As discussed in section 3.1, the beam forming method enhances the amplitude of a signal with a given slowness  $\mathbf{u}$ . As a prerequisite of this method all components of the slowness vector of the phase of interest must be known. To determine the unknown horizontal slowness or the back azimuth of an arriving signal, the so-called vespa process (velocity spectral analysis [Davies et al., 1971]) can be used. This method needs just one component of the slowness vector, horizontal slowness or back azimuth, as input.

[17] If a plane wave arrives at an array, the signal is recorded at the array stations with a certain time offset depending on the slowness vector of the wave and the position of the station in the array (equation (5)). These time delays are used to specify the slowness or back azimuth of the wave front, since they provide a direct estimate of the back azimuth and the slowness of the signal. The vespa combines the capability of beam forming to enhance the signal with the measurement of the slowness or back azimuth.

[18] The vespa in its original form [Davies et al., 1971] estimates the seismic energy arriving at the array for a given back azimuth and different horizontal slownesses  $u$ . Alternatively, the vespa process can be used for a fixed slowness and varying back azimuths. The result of the vespa process is displayed as a vespagram, a diagram of the energy content (amplitudes) of the incoming signals as a function of slowness or back azimuth and time. For a slowness vespagram calculated with varying slowness and for a fixed back azimuth, the beam traces of an array for the fixed back azimuth  $\theta$  are calculated by

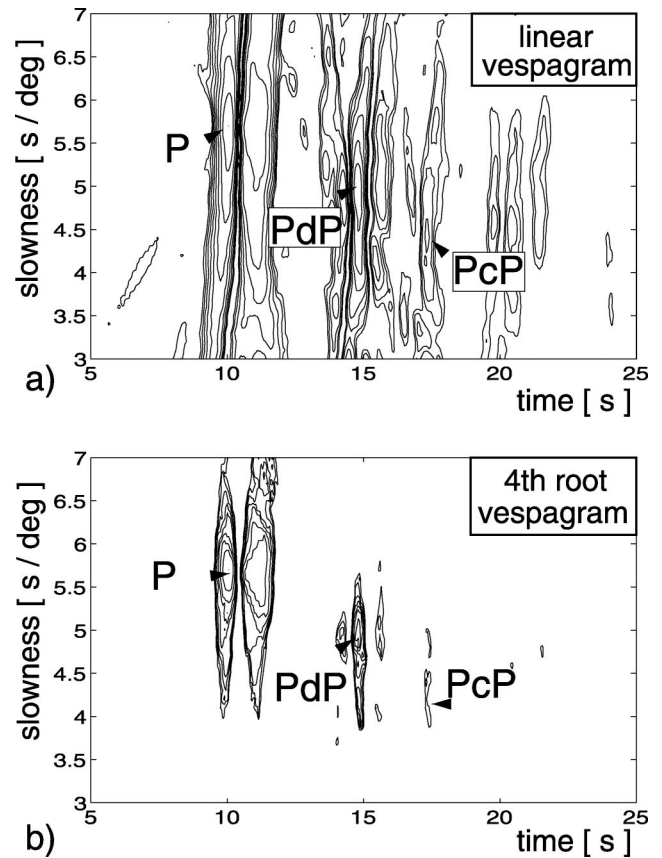


**Figure 5.** (a) Vespagram for the event of 17 December 1991 at 0638 UT (latitude 47.27, longitude 151.64, depth  $h = 154.1$  km, and  $m_b = 5.9$ ) in the Kurile region. The vespagram shows the energy recorded at the GRF and the German Regional Seismic Network (GRSN) for the theoretical back azimuth over time for varying slowness. The  $P$ ,  $PcP$ , and  $PdP$  (reflection of  $P$  wave at the  $D''$  discontinuity in the lowermost mantle) arrivals are marked.  $PdP$  and  $PcP$  show a slightly smaller slowness than  $P$ . (b) Fourth-root vespagram of the same event with better slowness resolution due to the fourth-root processing.

$$v_u(t) = \frac{1}{M} \sum_{i=1}^M x_i(t - t_{u,i}), \quad (9)$$

with  $x_i(t)$  representing the seismogram at station  $i$ ,  $t_{u,i}$  representing the relative travel time to station  $i$  for horizontal slowness  $u$ , and  $M$  representing the number of array stations.

[19] Owing to the different shift times according to different slownesses of the traces the method is also called slant stack. Figure 5a shows a vespagram of an earthquake located in the Kurile region recorded at the stations of the GRF and the German Regional Seismic Network (GRSN). Figure 5 shows the energy recorded as a function of time for different slownesses. The theoretical back azimuth ( $\theta = 26.6^\circ$ ) was chosen to produce this vespagram. The back azimuth was calculated between the source and the array center for the spherical symmetric Earth model of the International Association

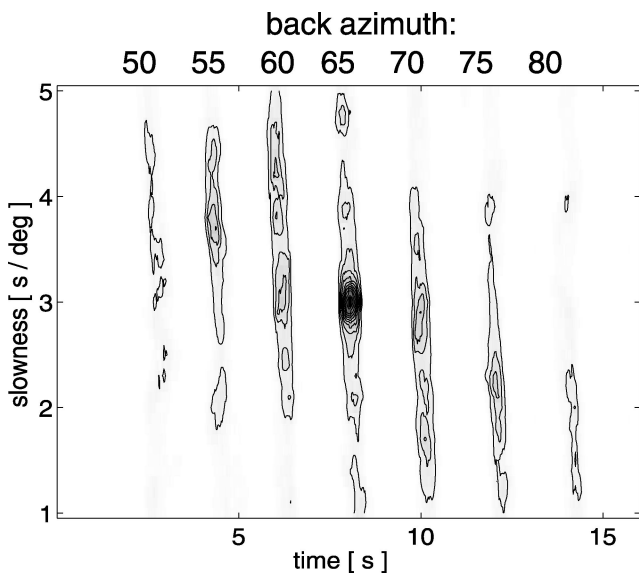


**Figure 6.** Example of a vespagram calculated using a wrong back azimuth. Synthetic data have been generated with a slowness of 3 s/deg and a varying back azimuth (from 50° to 80° in 5° steps, indicated by numbers above the phases). The fourth-root vespagram is calculated for a back azimuth of 65°. The slowness deviation for phases arriving with a back azimuth not equal to 65° is pronounced.

of Seismology and Physics IASP91 [Kennett and Engdahl, 1991]. In Figure 5 the slowness is shown in seconds per degree [s/deg]. One degree at the Earth's surface is  $\sim 111.19$  km and  $u$  [s/deg] =  $u$  [s/km] g with

$$g = \frac{\pi 6371 \text{ km}}{180^\circ} \cong 111.91 \text{ km}/^\circ. \quad (10)$$

In Figure 5 the time window around the  $P$  arrival is shown. The arrival times of  $P$ ,  $PcP$  (the reflection at the core-mantle boundary), and  $PdP$  are shown.  $PdP$  is a  $P$  wave reflected at the top of the D'' discontinuity  $\sim 300$  km above the core-mantle boundary (CMB) [Weber, 1993]. Often this phase is not visible in raw seismograms, and array processing is necessary to identify it.  $PdP$  is used to study the structure of the D'' layer above the CMB.

[20] The slowness resolution of this vespagram is poor and the expected small slowness differences (up to 1.3 s/deg) between  $P$ ,  $PdP$ , and  $PcP$  are not obvious. When calculating slowness (back azimuth) vespagrams, great care should be taken when selecting the appropriate fixed back azimuth (slowness). A wrong back azimuth (slowness) used for the computation may produce misleading slowness (back azimuth) measurements. A synthetic example of a slowness vespagram computed for a back azimuth of 65° is shown in Figure 6. The different phases in the seismograms used to compute this vespagram arrive with different back azimuths as marked at the top of the vespagram. The wrong back azimuth used for the calculation results in incorrect slowness readings.

[21] The underground beneath the array can affect

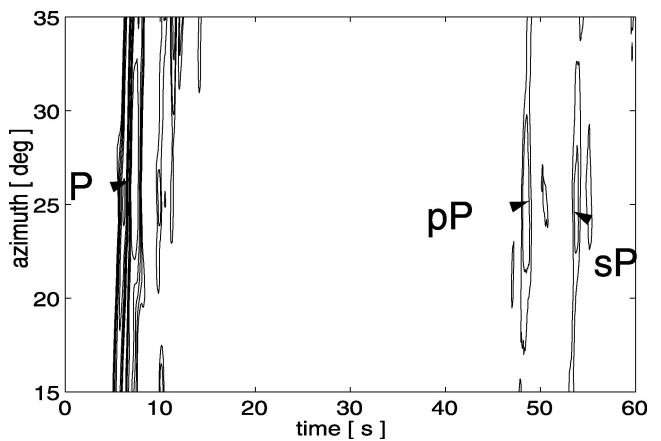


**Figure 7.** Example of a back azimuth vespagram. The same event as in Figure 5 was used. The time window includes the depth phases  $pP$  and  $sP$ . The phases  $P$ ,  $pP$ , and  $sP$  arrive along the theoretical back azimuth of 26°. The phases  $PdP$  and  $PcP$ , do not stack coherently because of their different slowness compared to the  $P$  slowness.

the back azimuth considerably because of the effect of structures directly beneath the array which may influence the time delays between the stations [Krüger and Weber, 1992]. Additionally, some phases in the teleseismic wave field may not arrive along the source-receiver plane. In these cases the use of the theoretical back azimuth may produce misleading results. The array underground also influences the slowness of different phases depending on the azimuth and the angle of incidence at the array. Therefore mislocation vectors exist for several arrays [Hwang and Clayton, 1991; Krüger and Weber, 1992] and should be used for the interpretation of measured phase slownesses and back azimuths.

[22] An example of a back azimuth vespagram is shown in Figure 7. The same event and the same stations as in Figure 5 have been used. As fixed slowness, the theoretical  $P$  slowness computed using IASP91 was used ( $u_P = 5.64$  s/deg). The  $P$  wave arrives with a back azimuth of  $\sim 26^\circ$ . The time window shown includes the depth phases  $pP$  ( $u_{pP} = 5.73$  s/deg) and  $sP$  ( $u_{sP} = 5.71$  s/deg) arriving along the same back azimuth as  $P$ . The phases  $PdP$  and  $PcP$  do not stack coherently because of the different slowness compared to the fixed slowness ( $u_{PdP} = 4.9$  s/deg and  $u_{PcP} = 4.3$  s/deg).

[23] The vespa process is a special case ( $N = 1$ ) of the  $N$ th root process, which is described in section 3.2.1. Therefore the “normal” vespa process is sometimes called linear vespa.

### 3.2.1. $N$ th Root Process

[24] As can be seen in Figure 5a, the slowness resolution of the linear vespagram is not always sufficient to separate arrivals with very similar slownesses. The  $N$ th-root vespagram [Kanasewich et al., 1973a; Muirhead and Datt, 1976; McFadden et al., 1986] can be used to enhance the slowness resolution.

[25] For the calculation of a  $N$ th-root vespagram, the  $N$ th root is extracted from the traces ( $N = 2, 3, 4, \dots$ ) before the summation of the individual array traces, while preserving the sign of each sample:

$$v'_{u,N} = \frac{1}{M} \sum_{i=1}^M |x_i(t - t_{u,i})|^{1/N} \frac{x_i(t)}{|x_i(t)|}. \quad (11)$$

After summation the beam trace is taken to the  $N$ th power, again the sign is kept:

$$v_{u,N}(t) = |v'_{u,N}(t)|^N \frac{v'_{u,N}}{|v'_{u,N}|}. \quad (12)$$

The  $N$ th root of the single-array traces reduces the amplitude differences of the samples, therefore reducing the amplitude variance of the trace. This means that coherent phases with smaller amplitudes have a bigger influence on the sum trace than in the linear vespagram. The  $N$ th power after the summation enhances the amplitude differences again. Owing to the smaller-amplitude differences in the trace after extracting the  $N$ th root, the coherence of a signal across the array is more important for a successful stack than high amplitudes of arrivals. Therefore the incoherent noise is suppressed very efficiently, whereas coherent phases are amplified and the slowness resolution is enhanced. Figure 5b shows a fourth-root vespagram with a significantly better slowness resolution than the linear vespagram in Figure 5a.

[26] The root function in equation (11) can be replaced by any nonlinear function  $f(x)$  if the function is monotonic and the inverse function  $f^{-1}(x)$  exists. A possible nonlinear function is, for example, the logarithmic function [Weichert, 1975]

$$f(x) = \log_a x \quad f^{-1}(x) = a^x. \quad (13)$$

The differences between the  $N$ th root and the logarithm are small, and normally only the  $N$ th-root function is used.

[27] The  $N$ th root process is nonlinear. The result of the nonlinearity is a distortion of the waveform of the signals [McFadden *et al.*, 1986] (Figure 8). This fact makes the  $N$ th-root process useless for waveform studies, although the wavelet polarity can be used because of the conservation of the sign of each sample (equation (11)).

### 3.2.2. Source Stacks

[28] The concept of combining clusters of sources in source arrays has long been known [Niazi, 1969]. Following the reciprocity theorem for Green's functions, the recordings of several seismic sources by a single instrument can be used in the same way as several recordings of a single source [Spudich and Bostwick, 1987; Scherbaum *et al.*, 1991]. The accuracy of the results depends, to a great extent, on the quality of the available

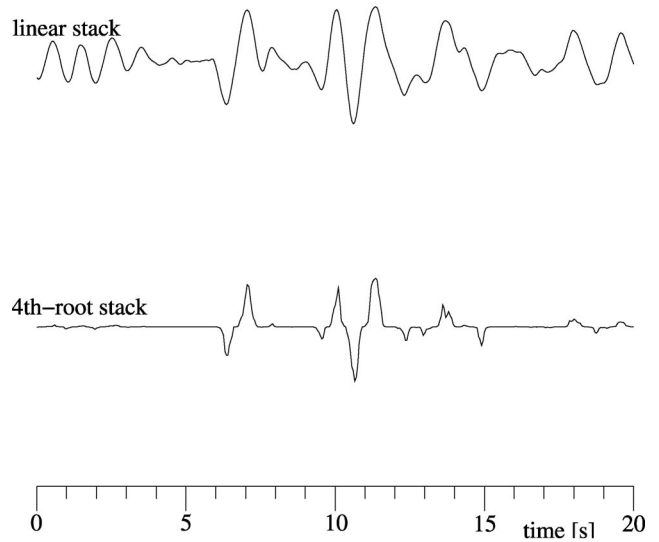


**Figure 8.** Signal distortion due to the nonlinear nature of the fourth-root process. The same event as in Figure 4 is shown. The time window around the  $pP$  and  $sP$  phases is selected. The top trace shows the trace for the  $P$  slowness (5.6 s/deg) of a linear vespagram. The bottom trace shows the corresponding fourth-root vesa trace with strong signal distortion. Note the reduced noise in the fourth-root beam trace.

information about the sources, such as location, origin times, and source mechanism.

[29] Source arrays are rarely used in global seismology because of the imprecisely known source parameters. In the past, arrays of nuclear explosions have mostly been used [Goldstein *et al.*, 1992] because the origin time and source location of nuclear explosions, in general, is well known. Additionally, explosions show simple and similar source mechanisms. To use earthquakes for source-array stacks, different normalizations must be applied, for example, for the source mechanism and the source depth. To overcome some of these problems, static origin time corrections can be applied to each seismogram [Krüger *et al.*, 1996]. The corrections assume that the waves approaching the source array propagate along great circle paths with a slowness  $u$  and add an additional time shift according to this slowness  $u$ . The source beam forming is then performed relative to  $u$ . Using these corrections, only relative slowness and back azimuth information of phases can be obtained [Krüger *et al.*, 1996; Thomas *et al.*, 2002].

[30] In analogy to the coherency requirement for the wave field in receiver array studies, the waveforms must be similar. In general, this requirement can be fulfilled by a source normalization method, such as a deconvolution with the source wavelet [Oldenburg, 1981]. Since the locations of receiver arrays are restricted to a limited number of places on the Earth, the regions in the Earth that can be studied are similarly restricted. Using source arrays, it is possible to construct arrays cheaply to study areas of the Earth that are not accessible with receiver arrays. An advantage of source arrays is the identical

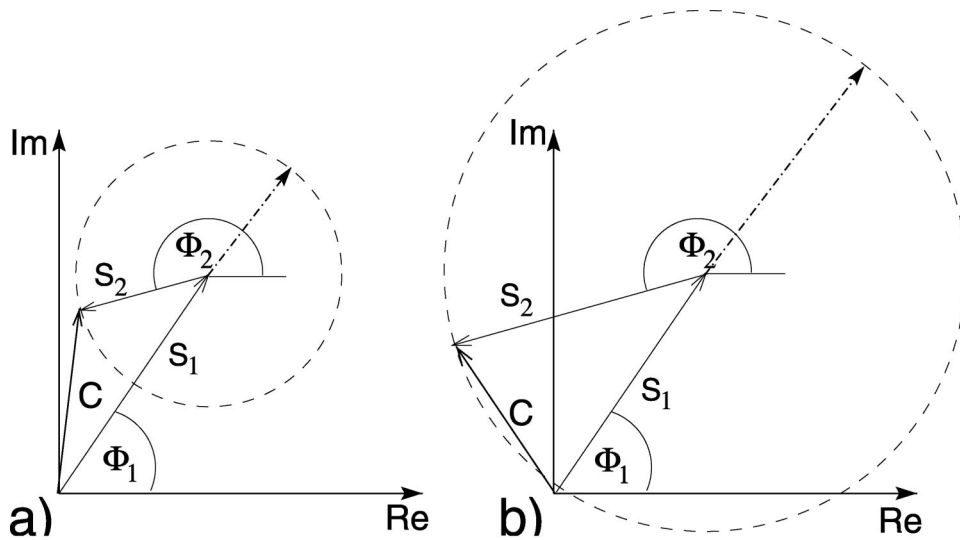


**Figure 9.** Illustration of the summation of two analytical signals  $S_1(t)$  and  $S_2(t)$  in the complex plane. (a) Non normalized summation. The sum vector  $C$  is not very sensitive to the instantaneous phase  $\Phi_2$  of  $S_2(t)$ . (b)  $S_1(t)$  and  $S_2(t)$  normalized on a sample-by-sample basis. This makes  $C$  very sensitive to changes of the instantaneous phase, so that  $|C|$  is a direct measurement of the coherency.

response of the recording instrument and the same subsurface beneath the station. A disadvantage, however, is that multiples from upper mantle discontinuities and other near-receiver structures are enhanced.

[31] The source array beam  $S_i(\mathbf{u}; t)$  for an arbitrary slowness vector  $\mathbf{u}$  is given by

$$S_i(\mathbf{u}, t) = \frac{1}{K} \sum_{k=1}^K a_k(t)^* x_{ik}(t - \kappa_k), \quad (14)$$

with

$K$	number of sources;
$a_k(t)$	source equalization factor;
$*$	convolution operator;
$x_{ik}$	seismogram of source $k$ at station $i$ .

[32] The form of equation (14) is identical to equation (5). The time delays are calculated by  $\kappa_k = (\mathbf{r}_k - \mathbf{r}_0)\mathbf{u}$ , where  $(\mathbf{r}_k - \mathbf{r}_0)$  describes the relative position of the event in the source array relative to a reference point  $\mathbf{r}_0$  or the location of a master event. The time delays  $\kappa$  may contain corrections for depth differences or source medium differences between events.

[33] All methods that can be applied to receiver arrays can also be applied to source arrays. Likewise, all errors included in receiver array studies must be taken into account with the restrictions discussed above. Source arrays are especially important in combination with receiver arrays as shown in the double-beam method described in section 3.4.

### 3.3. Phase-Weighted Stack

[34] The phase-weighted stack (PWS) method [Schimmel and Paulsen, 1997] is another nonlinear ar-

ray method to reduce incoherent noise in array recordings. PWS uses an amplitude-unbiased coherency measure to weight the samples of a linear stack.

[35] For PWS an analytical signal, or complex trace  $S(t)$ , is constructed from the seismic trace  $s(t)$ . The analytical signal contains the seismic signal  $s(t)$  as its real part and the Hilbert transform  $\mathcal{H}[s(t)]$  as its imaginary part:

$$S(t) = s(t) + i\mathcal{H}[s(t)] \quad (15)$$

This can be also expressed as amplitude  $A(t)$  and phase  $\Phi(t)$ :

$$S(t) = s(t) + i\mathcal{H}[s(t)] = A(t)\exp[i\Phi(t)]. \quad (16)$$

$A(t)$  is the envelope of the seismic trace  $s(t)$ , and  $\Phi(t)$  is called the instantaneous phase [Bracewell, 1965]. Equation (16) describes a vector with length  $A(t)$  which rotates with time in the complex space around the time axis.

[36] Two analytical signals are summed by vector summation (Figure 9) at a fixed time  $t = \tau$  on a sample-by-sample basis:

$$C(\tau) = S_1(\tau) + S_2(\tau). \quad (17)$$

The summation vector  $|C|$  will be maximum if the instantaneous phases  $\Phi_1$  and  $\Phi_2$  are equal, i.e., the two signals are coherent. For incoherent signals the amplitude  $|C|$  will be smaller. If the amplitudes of  $|S_1(\tau)|$  and  $|S_2(\tau)|$  differ, as is normally the case, and in case of large-amplitude noise, the summation vector  $|C(\tau)|$  can be larger for noise than for a small-amplitude coherent signal. This is accounted for by a sample-by-sample normalization of the two analytical traces (Figure 9b).

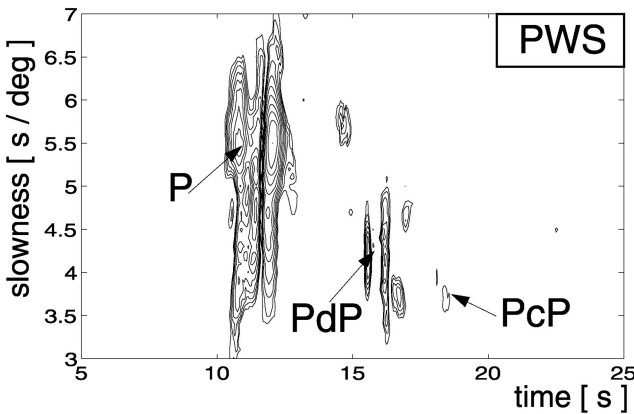


**Figure 10.** The fourth-power phase-weighted stack (PWS) of the example event shown in Figure 5. The influence of the power parameter on the resolution is higher than in the  $N$ th-root vespagram.  $N = 4$  for the vespagram is comparable to  $\nu = 3$  in the PWS [Jahnke, 1998].

The normalization makes  $|C|$  very sensitive to changes of the instantaneous phase and therefore very sensitive to the coherency of the two signals. With this it is possible to define a phase stack for a number  $N$  of traces:

$$c(t) = \frac{1}{N} \left| \sum_{j=1}^N \exp[i\Phi_j(t)] \right|, \quad (18)$$

with  $0 \leq c(t) \leq 1$ . Here  $c(t)$  measures the coherency of the input signals as a function of time, independent from the amplitudes of the input traces. For perfectly coherent signals,  $c(t) = 1$  and for incoherent noise  $c(t) = 0$ .

[37] The coherency measurement of equation (18) can now be used to weight the samples of a normal linear stack  $s_j(t)$  (equation (9)):

$$v_{\text{PWS}}(t) = \frac{1}{N} \sum_{j=1}^N s_j(t) \left| \frac{1}{N} \sum_{k=1}^N \exp[i\Phi_k(t)] \right|^{\nu}. \quad (19)$$

Equation (19) describes a phase-weighted stack. Every sample of the linear stack  $s_j(t)$  is weighted by the coherency of its instantaneous phases. The phase stack acts as a filter with respect to the similarity and dissimilarity of the signals. The sharpness of this coherency filter is controlled by the power factor  $\nu$ .

[38] As discussed above, PWS is a nonlinear technique, and the resulting signals will be distorted. An example for a fourth power PWS is shown in Figure 10. The influence of the power parameter  $\nu$  in PWS is larger than for the vespagram, so that  $\nu = 3$  is similar to  $N = 4$ . More tests and examples of this method are given by Schimmel and Paulsen [1997], where PWS was used to detect weak  $P$ -to- $S$  conversions from the mid mantle.

[39] PWS shows an improved slowness and time resolution because of the coherency weight compared to other slant stacking methods or coherency methods [Schimmel and Paulsen, 1997] at least for large arrays.

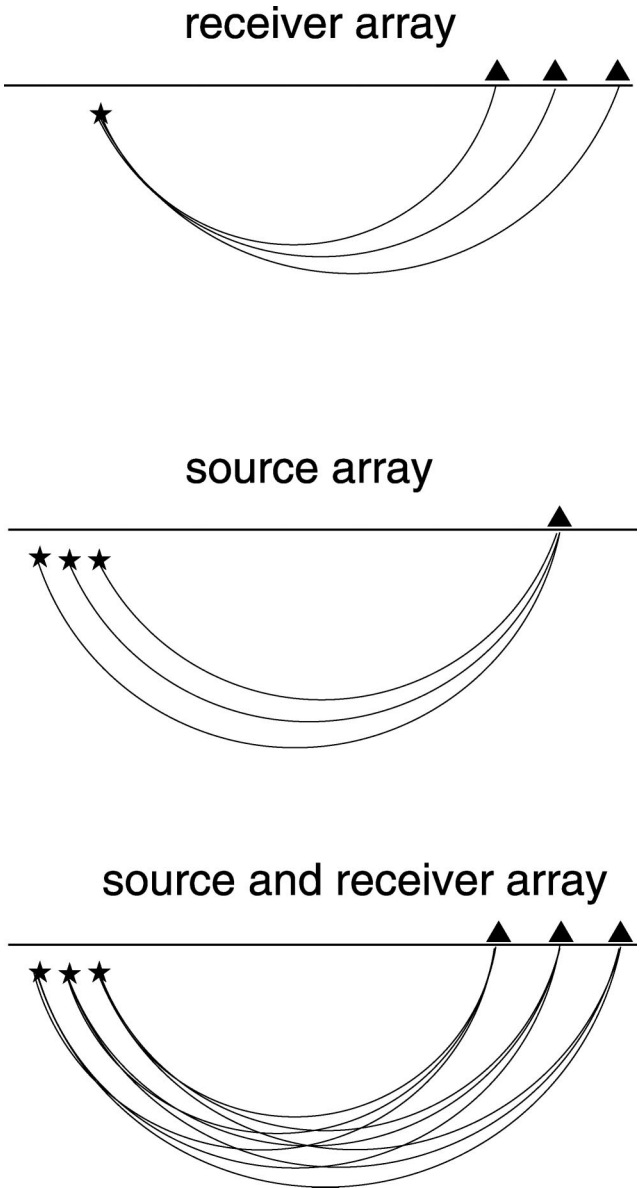


**Figure 11.** Principle of double beam. Stars denote sources; triangles are receivers. Compared to a single beam, the region where the rays turn is much better sampled by the double-beam method (source and receiver array).

For smaller arrays with a restricted slowness resolution the PWS seems to have no advantage over vespagrams.

### 3.4. Double Beam

[40] The double-beam method (DBM) combines source and receiver slant stacks to resolve Earth structure [Krüger et al., 1993, 1996; Scherbaum et al., 1997]. Combining source and receiver arrays leads to a better resolution of structures in the Earth's interior. The principle of the DBM is shown in Figure 11. Following equation (6), the receiver array beam for a receiver array with  $N$  stations and for a given slowness vector  $\mathbf{u}_r$  can be calculated by

$$R_k(\mathbf{u}_r, t) = \frac{1}{N} \sum_{i=1}^N x_{ik}(t + \mathbf{r}_i \cdot \mathbf{u}_r), \quad (20)$$

with  $x_{ik}(t)$  the seismogram of source  $s_k$  recorded at station  $\mathbf{r}_i$ .

[41] The source array beam for  $K$  sources (equation (14)) can be calculated by

$$S_i(\mathbf{u}_s, t) = \frac{1}{K} \sum_{k=1}^K a_k(t) * x_{ik}(t - \kappa_k). \quad (21)$$

Here  $a_k(t)$  is a source equalization factor which is necessary to normalize the wavelets of different sources by convolution. The time delays between the sources are calculated by  $\kappa_k = (\mathbf{s}_k - \mathbf{s}_0) \cdot \mathbf{u}_s$  for a certain slowness  $\mathbf{u}_s$ .

[42] The source and receiver configurations can be integrated to construct double beams. First, the source time delays  $\kappa_k = (\mathbf{s}_k - \mathbf{s}_0) \cdot \mathbf{u}_s$  are calculated for a certain source slowness vector  $\mathbf{u}_s$ , and for each station  $i$  of the receiver array the traces are delayed with  $\kappa_k$  and summed to form a source array beam  $S_i(\mathbf{v}, t)$  for a phase with slowness  $\mathbf{u}_s$ . In a second step the time delays  $\tau_i = (\mathbf{r}_i - \mathbf{r}_0) \cdot \mathbf{u}_r$  are calculated for each station  $i$  in the receiver array for a receiver slowness  $\mathbf{u}_r$ . The source array beams  $S_i$  are then delayed with  $\tau_i$  and summed to form the double beam:

$$D(\mathbf{u}_r, \mathbf{u}_s, t) = \frac{1}{I} \sum_{i=1}^I S_i(\mathbf{u}_s, t - \tau_i). \quad (22)$$

It is a special property of the double beam method to simultaneously obtain slowness information in the source region and at a distant array [Scherbaum *et al.*, 1997]. By steering the source and receiver array to selected target vectors  $\mathbf{u}_s$  and  $\mathbf{u}_r$ , it is possible to determine the slowness and back azimuth of wavelets at the receiver array in addition to their slowness and azimuth in the source region. The DBM has been used to map heterogeneities in the lower mantle [Scherbaum *et al.*, 1997; Krüger *et al.*, 1993, 1996] and the mid mantle [Krüger *et al.*, 2001] in great detail.

[43] The enhancement factor of the double-beam method in comparison to a receiver array is larger by a factor proportional to  $\sqrt{K}$ , with  $K$  as the number of sources used for the source beam forming (equation (14)) [Krüger *et al.*, 1996]. Since the DBM is a combined source and receiver slant stack, the problems of the individual methods transfer to the DBM.

### 3.5. Frequency–Wave Number Analysis

[44] In contrast to the array methods previously introduced, the frequency–wave number analysis (fk analysis) is able to measure the complete slowness vector (i.e., back azimuth  $\theta$  and horizontal slowness  $u$ ) simultaneously. The fk analysis calculates the power distributed among different slownesses and directions of approach

[Capon, 1973; Harjes and Henger, 1973; Aki and Richards, 1980]. As discussed in section 3.2, the time delays of the signals recorded at different array stations can be used for the analysis of seismic phases. The time delays required to bring the signals into phase provide a direct estimate of the back azimuth and the slowness of the signal. If the slowness and back azimuth of a signal are unknown, a grid search for all  $u$  and  $\theta$  combinations can be performed to find the best parameter combination, producing the highest amplitudes of the summed signal. This computation is performed in the spectral domain to save computation time.

[45] The following derivation of fk analysis follows Kelly [1967] and Harjes and Henger [1973]. A signal arriving at a reference point within the array with a horizontal velocity  $v_s$  and a back azimuth  $\theta$  is described as  $s(t)$ . The  $n$ th seismometer with the location vector  $\mathbf{r}_n$ , relative to the array reference point records the signal  $x_n(t)$ :

$$x_n(t) = s(t - \mathbf{u}_0 \cdot \mathbf{r}_n), \quad (23)$$

where  $\mathbf{u}_0$  is the slowness vector with

$$\mathbf{u}_0 = \frac{1}{v_0} (\cos \theta, \sin \theta), \quad (24)$$

where  $v_0$  is the surface velocity (equation (1)).

[46] The maximum amplitude of the sum of all array seismometers is reached if the signals of all stations are in phase, that is, if the time shifts  $\mathbf{u}_0 \cdot \mathbf{r}_n$  disappear (beam forming). The output of the array can be computed by

$$y(t) = \frac{1}{N} \sum_{n=1}^N x_n(t + \mathbf{u}_0 \cdot \mathbf{r}_n) \quad (25)$$

for an array of  $N$  elements. For a signal with a different slowness vector  $\mathbf{u}$  the beam trace is computed using equation (23):

$$y(t) = \frac{1}{N} \sum_{n=1}^N s \left\{ t + [(\mathbf{u}_0 - \mathbf{u}) \cdot \mathbf{r}_n] \right\}. \quad (26)$$

The total energy recorded at the array can be calculated by the integration of the squared summed amplitudes over time

$$\begin{aligned} E(k - k_0) &= \int_{-\infty}^{\infty} y^2(t) dt \\ &= \frac{1}{2\pi} \int_{-\infty}^{\infty} |S(\omega)|^2 \left| \frac{1}{N} \sum_{n=1}^N e^{2\pi i \cdot (\mathbf{k} - \mathbf{k}_0) \cdot \mathbf{r}_n} \right|^2 d\omega \end{aligned} \quad (27)$$

using Parseval's theorem. In equation (27),  $S(\omega)$  is the Fourier transform of  $s(t)$ , and  $\mathbf{k}$  is the wave number vector with

$$\mathbf{k} = (k_x, k_y) = \omega \cdot \mathbf{u} = \frac{\omega}{v_0} (\cos\theta, \sin\theta) \quad (28)$$

and  $\mathbf{k}_0$  is the wave number vector for  $\mathbf{u}_0$ . The back azimuth determines the direction of  $\mathbf{k}$  and the slowness the magnitude of  $\mathbf{k}$ . Equation (27) can be written as

$$E(\mathbf{k} - \mathbf{k}_0) = \frac{1}{2\pi} \int_{-\infty}^{\infty} |S(\omega)|^2 |A(\mathbf{k} - \mathbf{k}_0)|^2 d\omega, \quad (29)$$

with

$$|A(\mathbf{k} - \mathbf{k}_0)|^2 = \left| \frac{1}{N} \sum_{n=1}^N e^{(2\pi i(\mathbf{k} - \mathbf{k}_0) \cdot \mathbf{r}_n)} \right|^2 \quad (30)$$

as the array response function (ARF).

[47] As can be seen from equation (29), the total energy recorded at the array is defined by the power spectral density  $|S(\omega)|^2$  and the ARF  $|A(\mathbf{k} - \mathbf{k}_0)|^2$ . The ARF is controlled by the design (aperture, configuration, and interstation spacing) of the array.

[48] The result of the fk analysis is power spectral density as a function of slowness and back azimuth. The slowness can be calculated from the wave number vector  $\mathbf{k} = (k_x, k_y)$ :

$$|\mathbf{k}| = (k_x^2 + k_y^2)^{1/2} = \frac{2\pi}{u_s} = \frac{\omega}{v_s} \quad (31)$$

with  $u_s$  as the apparent horizontal slowness.

[49] The back azimuth  $\theta$  can be calculated by

$$\theta = \tan^{-1}(k_x/k_y). \quad (32)$$

The power spectral density is displayed in a polar coordinate system called the fk diagram. In the fk diagram the back azimuth is plotted on the azimuthal axis, and the slowness is plotted on the radial axis.

[50] The fk diagram is explained in Figure 12. Figure 13a shows the array response of the small-aperture Yellowknife array (YKA) in northern Canada (compare also Douglas [2002]). The ARF was computed for a monochromatic wave with a frequency of 1 Hz arriving at an array with YKA configuration. It has been assumed that the power spectral density  $S(\omega)$  is normalized:

$$\frac{1}{2\pi} \int_{-\infty}^{\infty} |S(\omega)|^2 d\omega = 1, \quad (33)$$

which leads to

$$E(\mathbf{k} - \mathbf{k}_0) = |A(\mathbf{k} - \mathbf{k}_0)|^2, \quad (34)$$

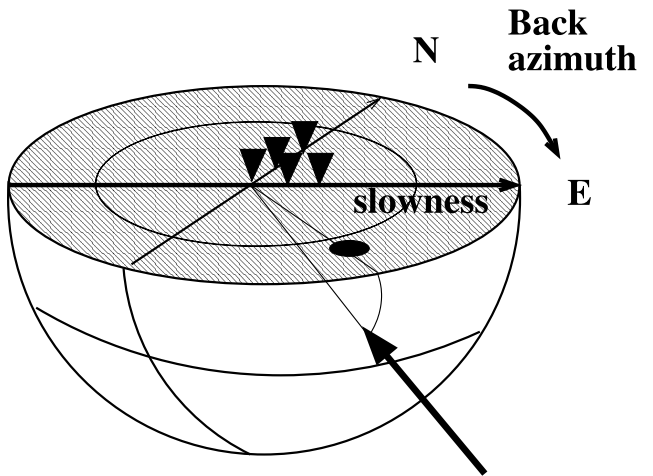


**Figure 12.** Explanation of the fk diagram. An incident wave travels through an imaginary half sphere beneath the array at point (X). The half sphere is projected to the surface in the fk diagram. The distance of the maximum energy from the origin gives the slowness; the angle from north gives the back azimuth.

where the wave arrives with a slowness  $u = 0$  (i.e.,  $\mathbf{k}_0 = 0$ ).

[51] For coherent waves with 1-s period arriving from different back azimuths and with slownesses different from  $u = 0$  s/deg, the maximum of the power spectral density is shifted to the corresponding values, without changing the form of the ARF. This is shown in Figure 13c for a signal arriving with a slowness of  $u = 7.5$  s/deg and a back azimuth  $\theta$  of 225°. For a signal arriving at YKA with different frequency  $f_1 \neq f_0 = 1$  Hz the fk diagram is scaled by the factor  $f_0/f_1$  without a change of the cross-shaped form of the ARF.

[52] For comparison, the array response function of the larger German Gräfenberg array is shown in Figure 14a. The larger aperture of 50 by 100 km and the different configuration result in a much better resolution for slowness and back azimuth than for the small-aperture Yellowknife array (Figure 13a).

[53] The fk analysis can only be applied to short time windows some seconds long. Large time windows may contain several different phases with different slowness vectors, which makes the unambiguous identification of a phase impossible. This implies that the fk analysis is best carried out using arrays for which the delay times of the arriving signal at all stations are small. This disadvantage can be avoided by careful selection of the time windows studied. As with most other array methods, the fk analysis assumes a plane wave front arriving at the array, small heterogeneities beneath the receivers can alter the wave front and destroy the coherency of the signals. This may change the results of the fk analysis.

### 3.6. Sliding-Window fk Analysis

[54] As discussed in section 3.5, the application of the fk analysis is restricted to short time windows. If the fk

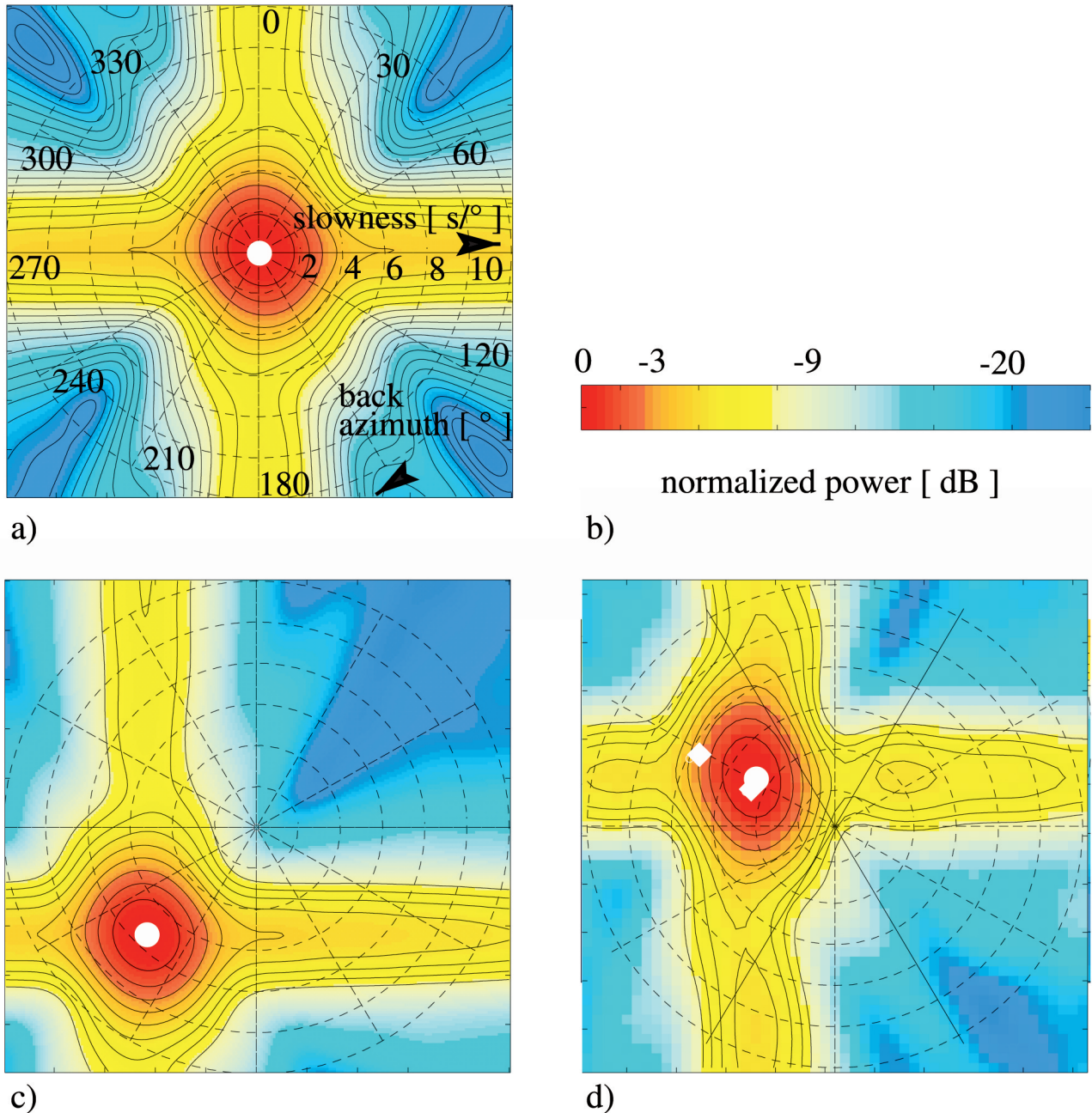


**Figure 13.** (a) Array response function of the small aperture Yellowknife array (YKA) computed for 1-Hz data. The logarithmic power spectral density is color-coded, and the maximum is normalized to 0 dB. The -1-dB isolines are added. The maximum power density is normalized to 0 dB (red). The slowness from 0 to 12 s/deg with 2 s/deg per tick is displayed on the radial axis; the back azimuth is shown clockwise from 0° to 360°. The slowness and back azimuth of the maximum power is marked by the white circle. (b) Power color scale for all fk diagrams. (c) Same as Figure 13a, but for a synthetic monochromatic (1 Hz) sinusoidal wave arriving at YKA with a  $u = 7.5$  s/deg and  $\theta = 225^\circ$ . For simplicity, fewer isolines are displayed in Figure 13c than in Figure 13a. (d) Same as Figure 13a, but for a  $P$  arrival of real data (event, 4 June 1993 at 1049 UT) at YKA. Theoretical slowness and back azimuth values are marked by the white diamonds. The lower diamond marks the  $P$  slowness ( $u_P = 4.43$ ). The other diamond marks the  $PP$  slowness ( $u_{PP} = 7.65$ ). The theoretical back azimuth is 295°.

analysis is applied to large time windows, the results are ambiguous. To avoid these restrictions and to analyze the development of slowness and back azimuth along the seismogram, the sliding-window fk analysis has been developed [Rost and Weber, 2001].

[55] In the sliding-window fk analysis a short time window of constant width is shifted along the seismogram with a constant step size, and a standard fk analysis is performed in every time window. The results of the fk analysis, i.e., the slowness and back azimuth of the power

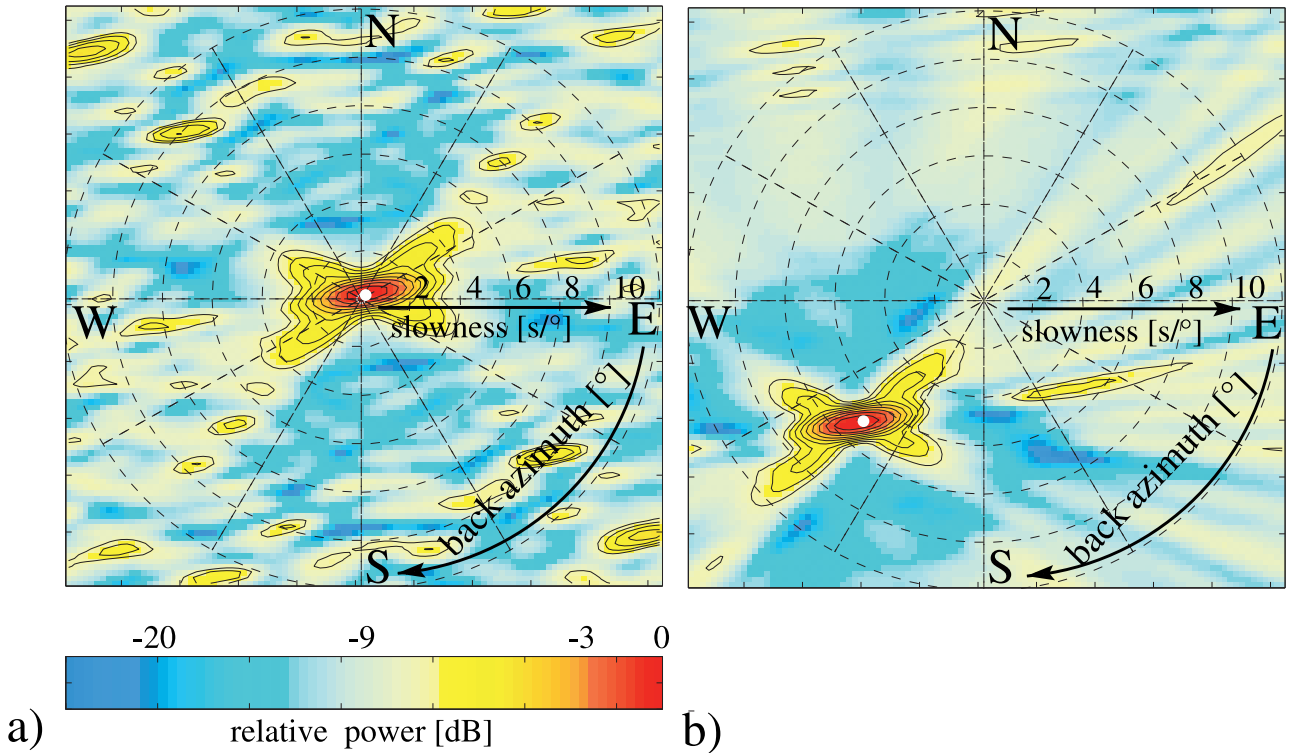


**Figure 14.** (a) Array response function of GRF. GRF has an aperture of  $\sim 50$  by  $100$  km. Owing to the larger aperture the resolution is higher than that of YKA (Figure 13a). (b) The fk analysis of a wave arriving with a slowness of  $7.75$  s/deg and along a back azimuth of  $225^\circ$ .

maximum and the information on the coherency of the signal for each time window, are stored. This transforms the array recordings into time series of coherency, slowness, and back azimuth.

[56] To obtain the best possible results in the fk analysis, a suitable time window and step size must be chosen. The time window must be wide enough to completely include phases traveling over the array with different slownesses. In shorter time windows, not all components of the signal can be analyzed, and the fk analysis becomes less accurate. If the window is too large, it will contain more incoherent noise, which disturbs the exact determination of slowness and back azimuth and, particularly, the coherency of the signal decays. Additionally, the time resolution of the method is reduced. The window width is defined by the dominant period of the signal and its travel time over the array. Therefore the appropriate window size is dependent on the size of the array and the slowness of the signals analyzed. The individual time windows should overlap somewhat to identify the continuous behavior of slowness and back azimuth, and the step size must be chosen accordingly.

[57] The sliding-window fk analysis is best used for small-aperture arrays with a well defined ARF that enables the identification of the arriving coherent signals. The sliding-window fk analysis has been applied in the search for *PP* underside reflections from upper mantle discontinuities [Rost and Weber, 2001]. The results of the

sliding-window fk analysis are displayed as fk movies. These movies give a good overview of the development of slowness and back azimuth along a seismogram. Some examples of the sliding-window fk analysis can be seen at <http://www.uni-geophys.gwdg.de/~srost/fk-movies.htm>.

### 3.7. Cophase

[58] The Cophase method is another method to enhance the signal strength and reduce noise and to estimate the signal phase velocity and direction [Posmentier and Herrmann, 1971]. Cophase was developed in the 1970s, when seismic analysis was restricted by limited computer power, as a rapid method to measure signal strength as a function of slowness and back azimuth. The results of Cophase are comparable to the fk analysis but with much less computational effort.

[59] Here we introduce the Cophase ad hoc processor to show a method completely defined in the frequency domain. The definition of Cophase is

$$C(V, \theta)$$

$$= \frac{\sum_{n=N_1}^{N_2} \sum_{j=k+1}^K \sum_{k=1}^{K-1} (A_j(\omega_n) + A_k(\omega_n)) \cos[(\Phi_j^F - \Phi_k^F) - (\Phi_j^V - \Phi_k^V)]}{\sum_{n=N}^{N_2} \sum_{j=k+1}^K \sum_{k=1}^{K-1} (A_j(\omega_n) + A_k(\omega_n))} \quad (35)$$

with

$V$	assumed phase velocity;
$\theta$	assumed back azimuth;
$n$	index of frequency;
$j$	detector number;
$\omega_n$	$n$ th frequency;
$A(\omega_n)$	$n$ th Fourier amplitude at the $j$ th detector;
$\Phi_j^F$	$n$ th Fourier phase at the $j$ th detector;
$\Phi_j^V$	phase of the $n$ th frequency at the $j$ th detector, based on the position of the detector and the assumed values of $V$ and $\theta$ .

[60] The value  $C(V, \theta)$  calculates the normalized weighted sum over all  $0.5K(K-1)$  detector pairs and over all frequencies of the cosines of the difference between the Fourier phase differences and the assumed phase differences.  $C(V, \theta)$  is 0 if the  $K$  records are uncorrelated and +1 if the  $K$  records represent a non-dispersive propagating signal with the expected values of  $V$  and  $\theta$ .

[61]  $C(V, \theta)$  is calculated from the Fourier transformed  $K$  records on a grid of slownesses and back azimuths. The grid point with the maximum signal  $C(V, \theta)$  is an estimate of the corresponding signal parameters.

[62] The most important limitations of the method are the intrinsic limitations of the array size and the array configuration. Additional limitations arise from the signal duration and the available bandwidth. The Cophase analysis per se does not show any important limitations [Posmentier and Herrmann, 1971]. Cophase was widely used in studies of the atmosphere with microbarograph arrays [Tolstoy et al., 1970].

### 3.8. Beaman

[63] Another processing method, which determines the slowness and back azimuth simultaneously in the time domain, was developed at Norwegian Seismic Array (NORSAR) and is described by King et al. [1976]. This technique is called beaman (beam power analysis) and was originally implemented for studying precursors to  $PP$  or core phases such as  $PKP$  and  $PKPPKP$  [King et al., 1975, 1976; Husebye and King, 1976; Haddon et al., 1977].

[64] An array beam for each nodal point on a defined slowness and azimuth grid is calculated, and the power distribution is analyzed as a function of time, azimuth, and slowness. This makes the method similar to the sliding-window fk analysis [Rost and Weber, 2001]. The power is estimated for each time interval (usually 1–2 s) by summing the squared beam amplitudes over groups of samples. The resulting contour plot is displayed in either the slowness–back azimuth plane or the slowness–time plane. Figure 15 shows a slowness back azimuth output for a precursor wave train to  $PKP$ .

[65] For NORSAR, which consisted of 22 subarrays, the intersubarray delay times were calculated for each grid point, but the intrasubarray time delays were calculated only for a group of  $7 \times 7$  grid points because of

computer capability limitations. For the analysis of precursors to  $PP$  or core phases this method was preferred over other methods, since it was able to deal with signals that persist over many cycles and variations of slowness and back azimuth along wave trains. Being able to resolve these variations is crucial for studying the causes of precursors [King et al., 1976]. Therefore beaman, which enhances time resolution, was used instead of, for example, the fk analysis, which enhances the frequency resolution. Also, beaman does not assume a fixed azimuth for the precursors as, for example, the vespa method does. Another reason to choose beaman came from the problems of other processing methods, which involved fitting a waveform to estimated slowness and back azimuth values to deal with interfering signals. In other words, these methods were not able to deal with precursors potentially caused by random medium scattering, although subarray structure also influences the results of beaman. Recently, a similar method (slowness–back azimuth analysis) was used by, for example, Weber and Wicks [1996] to analyze asymmetric reflections from a remnant subduction zone.

### 3.9. Migration

[66] Migration is a method borrowed from exploration geophysics, where it is used to move dipping reflectors into their true subsurface position, move diffraction effects back to their actual origin, or decrease the Fresnel zone. After Huygens's principle, a reflector is constructed by a series of point scatterers, each producing a diffraction hyperbola. These hyperbolae sum coherently only at the time of the main reflection; all other contributions do not sum coherently. However, if the reflector is finite, there will be a diffracted arrival from the endpoint that will show up in the data as an artifact, as a dipping, curved reflector. Migration can be used to project the energy back to its origin increasing the spatial resolution of the data [Yilmaz, 1987].

[67] In global seismology, migration was used to image heterogeneities in the Earth's mantle in a number of areas [Lynnes and Lay, 1989; Revenaugh, 1995; Bilek and Lay, 1998; Ying and Nataf, 1998; Thomas et al., 1999; Bostock and Rondenay, 1999]. These studies use different approaches that are, nonetheless, based on the same basic principles, and we will present a few of these approaches here.

[68] Lay [1987] and Lay and Lynnes [1989] have used teleseismic data to study near-source structures by using a coda migration technique: The traces are shifted and summed for a large number of sensors with shift times appropriate for scattered wave velocities and locations over a two- or three-dimensional grid. For a grid in the region of interest the time lags relative to the  $P$  wave for each source-receiver combination are calculated using

$$\tau_{ij} = \frac{r_i}{V_s} - \cos(\theta_i - \Phi_j)p_j r_i, \quad (36)$$

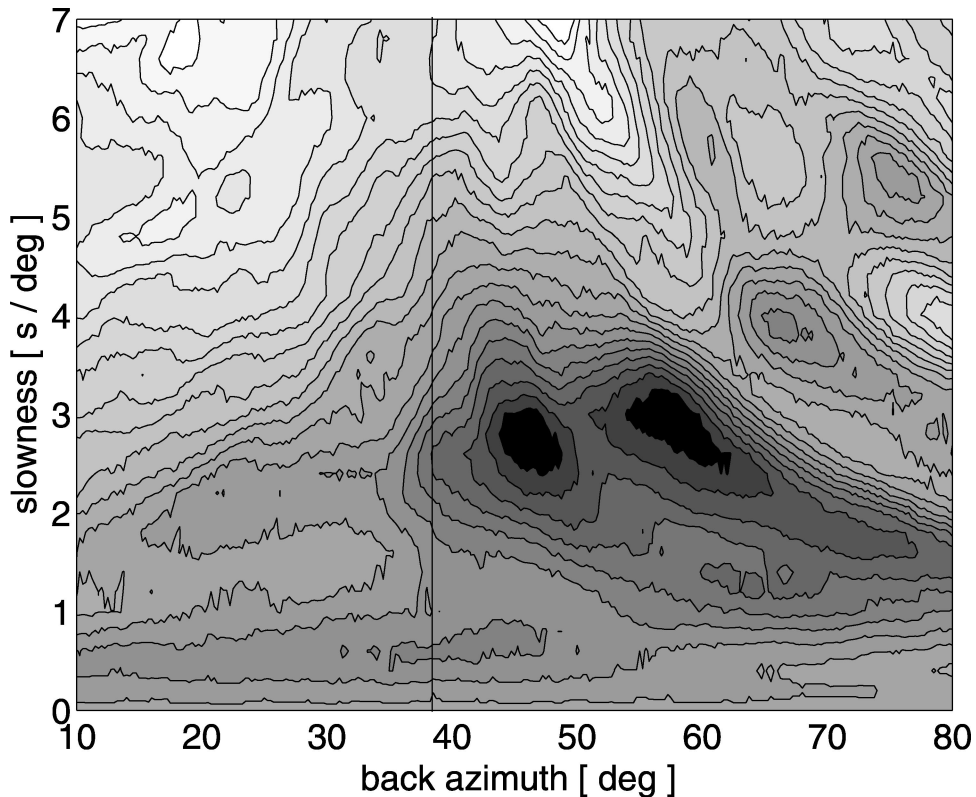


**Figure 15.** The results for the beaman technique applied to a precursor wave train ahead of the core phase PKP, recorded at four stations of the GRSN and the Gräfenberg array. Shown is the back azimuth–slowness plane. The maximum energy is indicated by the solid region. The theoretical back azimuth for the source-receiver combination is  $38^\circ$  (indicated by the solid line).

where the index  $i$  refers to the source-scatterer combination, the index  $j$  refers to the receiver,  $p_j$  is the horizontal ray parameter,  $\Phi_j$  is the azimuth from the sources to the receivers,  $r_i$  is the distance from each source to the scatterer with the corresponding azimuth  $\theta_i$ , and  $V_s$  is the velocity of the wave from the source which scatters into the  $P$  coda. With these lag times the slant stacks for each grid point can be computed, and the semblance [Neidell and Taner, 1971] can be calculated for a given time gate using

$$S(t_{ij}) = \frac{\sum_t^{t_g} \left[ \sum_i^{N_e} \sum_j^{N_s} f_{ij}(t + \tau_{ij}) \right]^2}{N_e N_s \left[ \sum_t^{t_g} \sum_i^{N_e} \sum_j^{N_s} f_{ij}(t)^2 \right]} \quad (37)$$

where  $N_e$  and  $N_s$  are the number of sources and receivers, respectively,  $f_{ij}$  is the recording of the  $i$ th event at the  $j$ th station, and  $t_g$  is the time gate. The semblance value gives the power of the stacked traces normalized with the total power in the seismograms. High semblance values (close to 1) indicate coherent waves. Comparable coda migration methods have been developed and applied by Hedlin *et al.* [1991] and Revenaugh [1995]. Following the coda migration method, Lay and Young

[1996] have proposed a similar form of migration [see also Bilek and Lay, 1998]. A scattering ellipsoid for each coda arrival is calculated, and the intersections with a grid are computed. Doing so for each source-receiver combination, some grid points may have more hits than others. The grid point with most hits is likely to be the scattering point for the specific coda phase.

[69] A similar approach has been introduced by Scherbaum *et al.* [1997]. The difference in their double-beam stack migration compared to other migration methods described here is that, in addition to using source and receiver arrays simultaneously, they also utilize back azimuth and slowness information at the source and receiver arrays.

[70] Applying the migration method to scattered teleseismic waves, Thomas *et al.* [1999] have followed an approach similar to Lay [1987] and Lay and Lynnes [1989] placing grids into the region of interest and treating each grid point as a secondary source. For each grid point the travel time to each station is calculated (i.e., parts of the diffraction hyperbola). The traces are then back shifted with these travel times for each grid point and stacked. The maximum amplitude within a time window around the theoretical arrival time of the phase of interest for a reference station can be determined, and the result can be mapped onto the corresponding

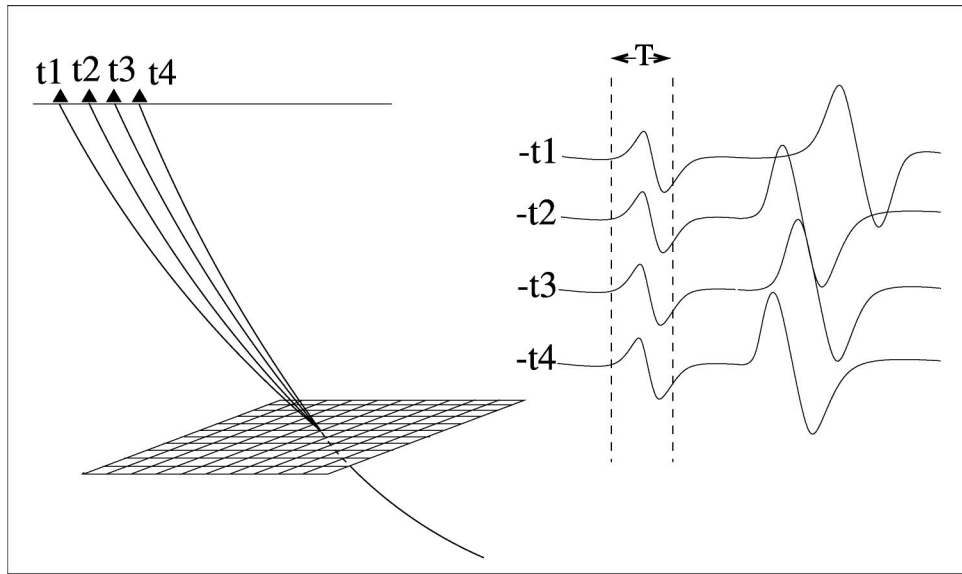


**Figure 16.** The migration method used by Thomas *et al.* [1999]. From a grid in the region of interest, travel times from each grid point to each station are calculated ( $t_1$  to  $t_4$ ), and the traces of the seismogram section are back shifted with these travel times. The traces are summed, and the maximum amplitude of the sum trace in a time window around the theoretical arrival time of the phase produced (i.e., scattered or reflected) at this grid point is determined and assigned to the grid point.

grid point (Figure 16). For only one source and receiver the energy would be distributed along one isochrone, but if an array is used, the region where the scattered phase originates can be narrowed down, since the arrival times at different stations differ for all grid points. Figure 17 shows the result for a layer 1 km above the CMB for a migration of scattered waves back to the lowermost mantle. This shows that it is possible to find the exact

location of very small features deep inside the Earth when using array methods.

[71] Recently, the classical migration has become important to teleseismic array studies for studying upper mantle discontinuities by applying it to receiver functions constructed from array recordings. An example is the pseudostation method as described by Neal and Pavlis [1999, 2001], in which conventional array beamforming methods are combined with receiver function analysis.

[72] In addition to the advantage that the migration method can be applied to waves where the plane wave approximation cannot be assumed, it also offers a possibility of projecting scattered or reflected waves back to their origin. However, one has to keep in mind that when using recordings from a large array, reflection points for a reflected phase will not be the same for each station, and therefore a larger area will show higher stacked amplitudes depending on the “footprint” of the array on the reflector. The resolution of the migration depends on the chosen grid, with the limits of resolution due to computational costs. When studying phases with a small slowness (e.g., core phases), i.e., with a steep incidence angle, the depth resolution of the migration method will be poorer compared to phases with a larger slowness, because the delay times between the stations will not differ much for different depths, given steep angles of incidence of a phase.

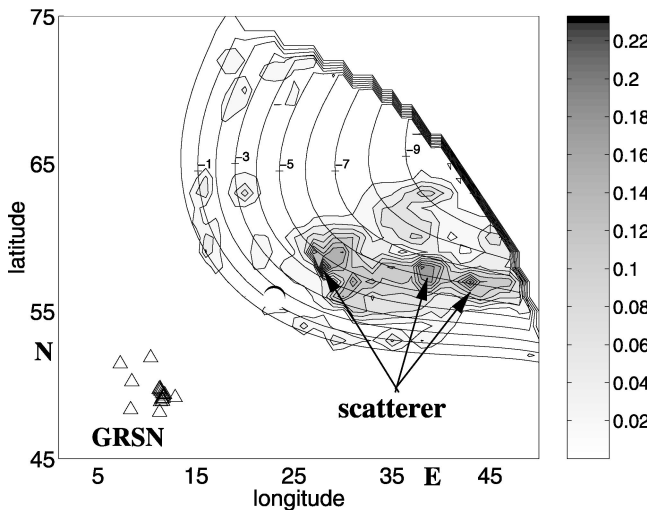


**Figure 17.** Example of a result of a migration of scattered waves in the lowermost mantle. Shown are isochrones (solid lemon-slice-shaped lines) and the most likely location of scatterers at a layer 1 km above the core-mantle boundary on a rectangular grid. The location of the stations of the GRSN are shown as triangles. The shading scale gives the maximum amplitude of the stacked traces.

### 3.10. Three-Component Arrays

[73] With the increasing use of digital three-component seismometers, three-component stations are used

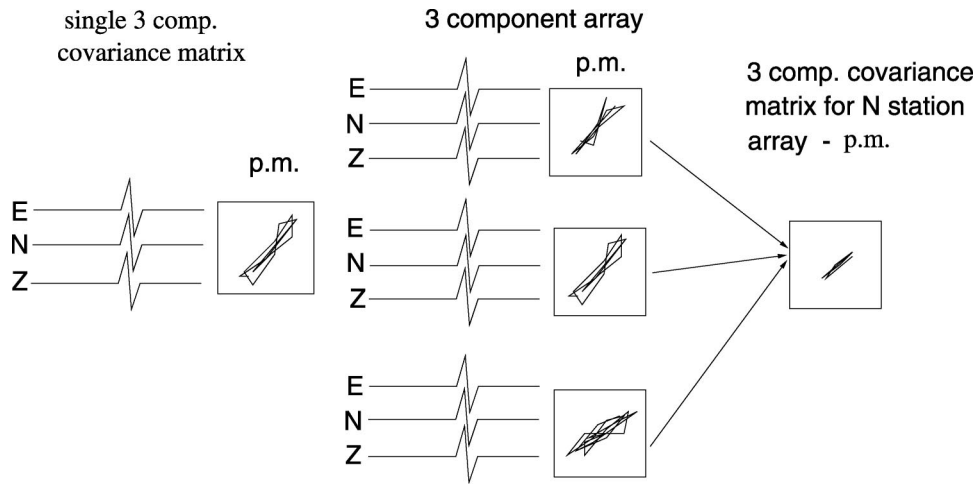


**Figure 18.** The principle using a three-component array for particle motion studies. For a single three-component station the covariance matrix describes the characteristics of the particle motion. For an array of three-component stations the mean of the covariance matrices of all stations is calculated. The resulting particle motion shows a smaller variance than the individual stations, and the characteristics of the motion as described in the text can be determined with smaller errors.

more and more in array configurations [Kvaerna and Doornboos, 1986]. Some of the permanent arrays are now equipped completely or partly with three-component stations, and more frequently temporary arrays follow the same trend.

[74] Three-component arrays can be used for different purposes than one-component (mostly vertical) array deployments, and the methods used also differ. Single three-component stations are unable to unambiguously separate superimposed signals and noise, but they can be used to determine the wave types of the recorded signals. One-component vertical arrays, however, can measure the slowness vector of incoming waves and are able to separate superimposed signals and noise. The disadvantage of one-component vertical arrays is, however, that significant portions of *P*, *SV*, and Rayleigh waves and the entire *SH* and Love wave part of the wave field are missing. The additional spatial information which is gained by a three-component seismic array allows us to isolate and estimate both the propagation direction and apparent velocity of coherent signals prior to the polarization analysis in order to separate and distinguish between different phases. Three-component arrays were used widely in analyses of *P* wave coda, scattering, and the study of regional wave propagation [Jurkevics, 1988; Dainty, 1990; Wagner and Owens, 1993; Kuwahara *et al.*, 1997; Wagner, 1997; Bear *et al.*, 1999].

[75] Here we introduce one example of a method to measure the polarization ellipse with a three-component array as shown by Jurkevics [1988]. The polarization ellipse is computed within sliding time windows by solving the eigenproblem for the covariance matrix. The data are filtered in narrow frequency bands, and the polarization ellipse is calculated in each time window

and each band (Figure 18). For a single three-component station the covariance matrix  $\mathbf{S}$  is evaluated by

$$S_{jk} = \frac{\mathbf{X}\mathbf{X}^T}{M} = \left[ \frac{1}{M} \sum_{i=1}^M x_{ij}x_{ik} \right], \quad (38)$$

with the data matrix  $\mathbf{X} = [x_{ij}]$ , where  $i = 1, \dots, M$  and  $j = 1, \dots, 3$ . Here  $x_{ij}$  is the  $i$ th sample of component  $j$ , and  $M$  is the number of samples. In other words, the terms of  $\mathbf{S}$  are the auto variances and cross variances of the three components of motion:

$$\mathbf{S} = \begin{bmatrix} S_{zz} & S_{zn} & S_{ze} \\ S_{zn} & S_{nn} & S_{ne} \\ S_{ze} & S_{ne} & S_{ee} \end{bmatrix}, \quad (39)$$

where  $S_{zn}$  denotes the cross variance of the vertical and north components, etc. The principal axes of the polarization ellipsoid are found by solving the eigenproblem for  $\mathbf{S}$ , finding the eigenvalues ( $\lambda_1, \lambda_2, \lambda_3$ ) and the corresponding eigenvectors ( $\mathbf{u}_1, \mathbf{u}_2, \mathbf{u}_3$ ) by finding nontrivial solutions to

$$(\mathbf{S} - \lambda^2 \mathbf{I})\mathbf{u} = \mathbf{0}, \quad (40)$$

where  $\mathbf{I}$  is the 3 by 3 identity matrix and  $\mathbf{0}$  is a column vector of zeros.

[76] From the principal axes of the polarization ellipsoid the particle motion can be determined, and information about the characteristics of the ground motion can be extracted. The azimuth of the *P* wave can be estimated from the horizontal orientation of the rectilinear motion given by eigenvector  $\mathbf{u}_1$ , the corresponding eigenvector to the largest eigenvalue

$$\theta_P = \tan^{-1} \left( \frac{u_{21} \text{sign}(u_{11})}{u_{31} \text{sign}(u_{11})} \right) \quad (41)$$

where  $u_{j1}, j = 1, \dots, 3$ , are the three direction cosines of  $\mathbf{u}_1$ . Similarly, the incident angle  $i$  can be determined:

$$i = \cos^{-1} |u_{11}|. \quad (42)$$

For the evaluation of the polarization matrix with a three-component array the method of *Jurkevics* [1988] calculates the average of the covariance matrix  $\mathbf{S}$  of all array stations. The principle of the method is shown in Figure 18. The use of several array stations reduces the variances of the ground motion characteristics. The three-component array covariance matrix for an array with  $N$  three-component stations is

$$\bar{\mathbf{S}} = \frac{1}{N} \sum_{n=1}^N \mathbf{S}_n, \quad (43)$$

where  $\mathbf{S}_n$  is the covariance matrix for sensor  $n$ . The estimation variance of the covariance matrix is reduced by a factor of  $1/N$  when using  $N$  array stations [Jurkevics, 1988].

[77] To use the average of the single-array station covariance matrices rather than the covariance matrix of an array beam trace eliminates timing errors. Particle motion estimates are very sensitive to timing errors between the components of motion. When the beam forming is performed first, the covariance matrix includes cross terms between the different stations, and the time alignment between sensors must be very accurate. For the covariance averaging it is only necessary to remove the time shifts between the stations due to the slowness of the arriving wave front. However, the accuracy required is much less than that needed for the beam forming [Jurkevics, 1988]. Using different time offsets, it is possible to steer the array and therewith to separate different wave types to study them individually.

[78] Different approaches exist to evaluate the polarization matrix. For more detailed descriptions of these methods we refer the reader to the existing literature [e.g., *Wagner and Owens*, 1993; *Wagner*, 1997; *Bear et al.*, 1999].

## 4. ARRAYS

### 4.1. Overview

[79] Although there is no strict definition of a seismological array, the minimum requirements are three or more identical instruments with a proper spacing, dependent on the noise and signal properties, centralized data acquisition, and integrated real-time processing. Modern array seismology came into being in 1957 as a test to detect underground nuclear explosions [*Husebye and Ruud*, 1989]. This test showed that the only effective way to detect underground explosions is by seismic means.

[80] The essential capability to locate the source of the incoming signal is the resolution of the signal in the

frequency–wave number space, which designates a certain ray path in the Earth and the source location. Different methods to resolve these wave parameters were discussed in sections 3.1–3.8.

[81] Since the beginning of seismic monitoring of nuclear explosions the need for reliable nuclear explosion monitoring and array seismology have been closely connected. As a result of these needs, several countries started research projects to install seismological arrays and to develop the necessary array methods. The arrays can be classified by their aperture, the instrument spacing, and the number of array stations. Some arrays and array types are discussed in section 4.2, and we use the size of the array or the aperture as discrimination.

[82] Different array designs have been tested in the past, and, depending on the application of the array, their geometries vary significantly. Some principal conditions should be met for a good seismological array. The ARF should have a sharp main lobe, ideally a  $\delta$  pulse with a strong suppression of the energy next to the main lobe. Additionally, the sidelobes due to spatial aliasing should not be within the wave number window of interest. These prerequisites depend on the wavelength of the phase studied. Therefore seismological arrays are built with respect to a certain frequency content of the main phase studied. To fulfill these criteria, the number of array stations, the interstation spacing, and the configuration of the array can be varied. The aperture of the array affects the sharpness of the main lobe, i.e., the ability of the array to separate the wave numbers of two incoming wave fronts. This is the resolution of the array. The number of sites controls the suppression of energy crossing the array at the same time with a different slowness, i.e., the quality of the array as a wave number filter. The interstation spacing of the array stations defines the position of the sidelobes in the ARF and the largest resolvable wave number; that is, the smaller the interstation spacing, the larger the wavelength of a resolvable seismic phase will be. Finally, the geometry of the array controls the azimuthal dependency of the resolution and the quality and the position of the sidelobes [*Harjes and Henger*, 1973]. An ideal array would show a Dirac  $\delta$  pulse as ARF. The slowness of the incoming signal can then be measured perfectly, energy arriving with a different slowness is suppressed perfectly, and the resolution does not change with different azimuths. This perfect array can be approximated by a circular array with irregular spacing of the array stations [*Haubrich*, 1968; *Harjes and Henger*, 1973; *Mykkeltveit et al.*, 1983].

### 4.2. Array Types

[83] This section discusses several arrays and shows some of the advantages and disadvantages of the different configurations. The presented arrays make up only a small portion of all array installations in use over previous years, and the selection is highly biased by our own usage of data sets of these arrays.

#### 4.2.1. Large and Medium-Sized Arrays

[84] The group of large arrays contains arrays like the Norwegian Seismic Array (Norway) and the large-aperture seismic array (LASA) (United States), with several hundreds of stations and an aperture of up to 200 km. LASA was built in 1965 with a total of 630 short-period and long-period digital seismometers [Frosch and Green, 1966; Husebye and Ruud, 1989]. The LASA recordings are still partly used today for seismological research [Vidale *et al.*, 2000; Earle, 2002] after a data rescuing effort [Hedlin *et al.*, 2000].

[85] The array was configured in 21 subarrays, which were arranged on circles with increasing radius. Each of these subarrays comprised 25 short-period instruments plus one three-component long-period instrument. The subarrays had apertures of 7 km, and the seismometers were grouped on concentric circles with a spacing of 0.5 km. LASA was built solely for the monitoring of nuclear explosions. Owing to the large overall aperture of the array and the small interstation spacing within the subarrays, there were problems with noise and signal coherency. Over the whole array the transient signals were no longer coherent, whereas the noise was still coherent between subarray stations. To ensure the noise incoherency, about nine out of 25 sensors were removed from each subarray to obtain a sensor spacing of 2–3 km [Mykkeltveit *et al.*, 1983].

[86] After some years of operation it became clear that a few large arrays are not able to globally monitor underground nuclear testing [Husebye and Ruud, 1989]. Because of this inability and funding problems, LASA was closed down in 1978.

[87] The second huge seismological array is NORSAR, with an aperture of ~100 km located in Norway. The array used to consist of 22 subarrays grouped in circles. Every subarray consisted of six short-period and one three-component long-period instrument. For the same reasons that LASA was closed down, NORSAR was reduced in size. The present configuration consists of seven subarrays with an aperture of ~70 km.

[88] Both array locations, their configuration, and the subarray configuration can be seen in Figure 19, with NORSAR shown in its former configuration, i.e., before size reduction. These arrays were mainly used to record teleseismic events in the frequency range of 1.0–2.5 Hz. Local and regional events could not be used because of the poor signal correlation, a result of the large aperture of both arrays. Another shortcoming of the large arrays was the varying signal amplitude at the subarrays. Because of the large extent of the arrays the amplitude response is highly selective in terms of angle of incidence of the incoming wave front [Husebye *et al.*, 1974]. Owing to this effect, using only some of the best subarrays for the studies showed equally good results as the analysis of the whole array, making the high costs for huge arrays unnecessary. This shows that arrays of this size are not

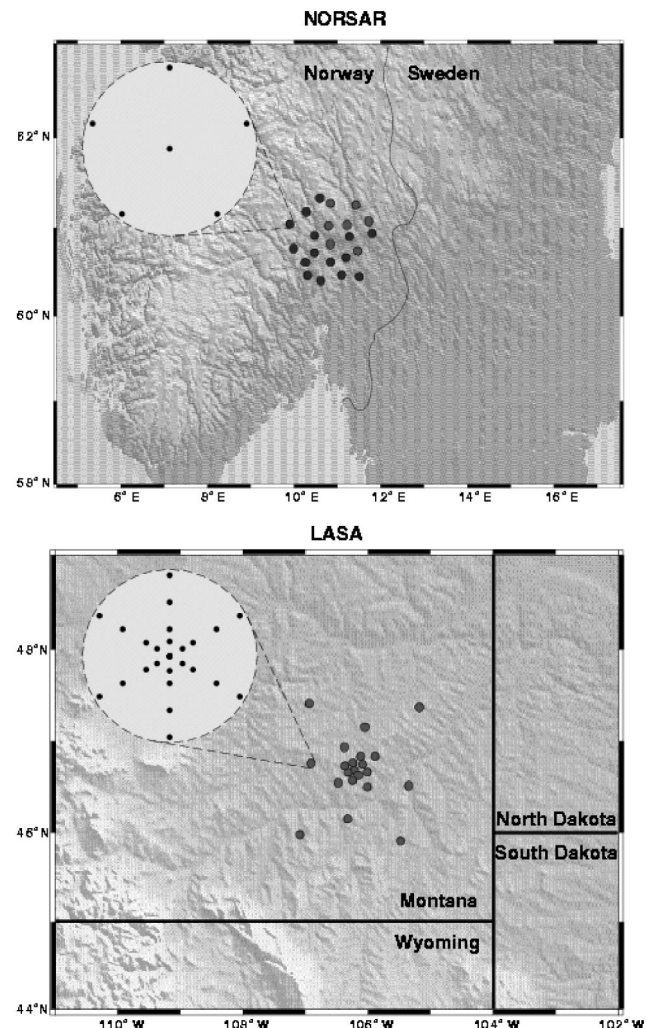


**Figure 19.** Location and configuration of the two large arrays, Norwegian Seismic Array (NORSAR) (Norway) and large-aperture seismic array (LASA) (United States), discussed in the text. The insets show the configuration of the subarrays. Note the reduction of subarray stations between LASA and NORSAR, which was necessary because of coherent noise conditions at subarray stations. Figure 19 is from Hedlin *et al.* [2000].

well suited for providing the best possible performance for the detection of teleseismic signals.

[89] A second class of seismic arrays, the medium-sized arrays, was introduced in the mid 1970s. An example of this, the Gräfenberg array, located in the Frankonian Jura, Germany, is exceptionally built to follow a homogeneous geological setting and shows good noise conditions because of low population, little industry, and low traffic density (Figure 20). Compared to NORSAR and LASA, the shape is irregular and follows the chalk plateau of the Frankonian Jura to provide a geology as homogeneous as possible beneath the array stations. This setting provides a database with high spatial coherence of signals but with low seismic noise. The first data from GRF are available from 1976; the array became fully operational in 1980. The final configuration consists

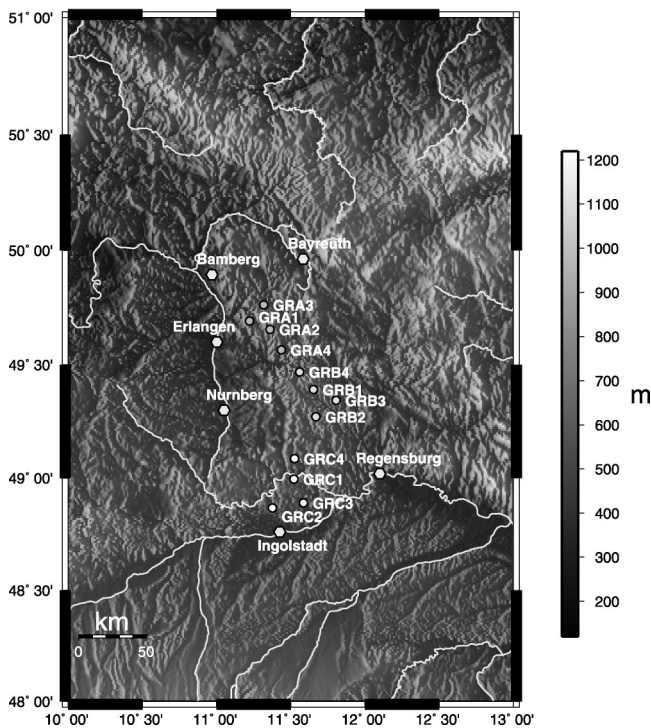


**Figure 20.** Location of the array stations of the GRF array. The circles represent the location of one-component vertical STS-1 broadband seismometers. Three of the stations (GRA1, GRB1, and GRC1) are equipped with three-component STS-1 seismometers. Topography data are from *Hastings and Dunbar* [1998].

of 13 broadband seismic stations (STS-1 seismometers [*Wielandt and Streckeisen*, 1982]), three of which are three-component stations, that cover an area of  $100 \times 50$  km with an average station spacing of 15 km in an L-shaped configuration. The GRF array was the first continuously registering broadband array and combined the advantages of array seismology, modern broadband sensors, and the possibility of digital recording [*Buttkus*, 1986].

#### 4.2.2. Temporary Arrays or Networks

[90] In recent years the deployment of temporary arrays has improved our knowledge of the structure of the Earth's interior tremendously. Owing to the large number of experimental arrays a discussion of all these experiments is beyond the scope of this paper.

[91] Temporary arrays are mostly built to suit one specific purpose so they target one specific research topic. Most experiments focus on the study of the crust, lithosphere, and upper mantle, but the teleseismic data can also be used for studies of Earth's deep interior. It is possible to divide the temporary array deployments into two large groups: (1) linear arrays which are best suited to study the layered structure of the Earth, especially in the upper mantle beneath the array; and (2) clustered arrays, where stations are deployed as a dense network, which are often used for regional tomographical studies.

[92] The First group of linear arrays is very popular since they are easy to deploy and to service even in regions of the Earth difficult to access because they can be deployed along roads. One of the more recent deployments is the Missouri to Massachusetts Broadband Seismometer Experiment (MOMA). For this experiment, seismometers were deployed for 1 year in 1995 and 1996 along a 1740-km-long line from Missouri to the permanent station HRV (Cambridge, Massachusetts) [*Wysession et al.*, 1996]. This experiment is exceptional because its data were used to address numerous scientific questions, ranging from upper mantle structure [e.g., *Al-Eqabi et al.*, 1996] to structure at the core-mantle boundary [e.g., *Wysession*, 1996]. Other arrays in this group include the Florida to Edmonton array, a 15-month deployment (2001–2002) of 28 stations across much of North America between Florida and Edmonton (Alberta, Canada), built to study the core-mantle boundary, D'', and the crust and upper mantle of North America; the Teleseismic Western Superior Transect array, in which 11 short-period three-component and 14 broadband three-component seismometers were deployed along a 600-km line in Ontario (Canada) [*Kay et al.*, 1999]; and the Seismic Profile of the Inner Core and D'' (SPICeD) array with stations in Scotland, England, and France that was built to study the Earth's deep interior [*Helffrich et al.*, 2002]. These are just a few arbitrary examples from many similar experiments. Linear arrays suffer from several shortcomings. The most important may be the lack of slowness resolution for waves arriving with back azimuths perpendicular to the strike of the array. This problem can be reduced by pointing the strike of the array toward a dominant source of seismicity as has been done for MOMA and SPICeD. Another problem arises from the size of these arrays, which results in a lack of coherency of waveforms along the array. Owing to the lack of crossing paths, linear arrays cannot be used to infer the lateral variations of seismic velocities by tomography. Dense clusters of stations are better able to resolve the fine-scale velocity structure beneath the array. One example of a high-density array for high-resolution tomography is the Eifel Plume Project (1997–1998) [*Ritter et al.*, 1998, 2001], where 158 mobile stations were deployed with an aperture of  $500 \times 500$  km in the Eifel region in western Germany to resolve the origin of recent Eifel volcanism. Besides the tomography part the project involves receiver function studies, anisotropy studies, and geochemical and magnetotelluric studies. A similar European array deployed to study the lithosphere and asthenosphere in northern Europe by tomography is Teleseismic Tomography of the Tornquist Zone project, where 120 broadband and short-period instruments were deployed from Germany through Denmark to Sweden [*Griegersen et al.*, 1999; *Arlitt et al.*, 1999]. To analyze the structure of the mantle, information from previous refraction profiles in the region has been used to set up a three-dimensional crustal structure model.

[93] In the period of 1993–1998 a new array form was tested in Australia. The SKIPPY project uses a series of deployments of up to 12 seismometers for periods of five months at a time. The deployments moved across Australia in a 5-year period [van der Hilst, 1994; Kennett and van der Hilst, 1996]. The different deployments can be combined to form a synthetic array covering the whole continent with an interstation spacing of  $\sim 400$  km. The data have been widely used for surface wave tomography because of the seismicity that surrounds Australia [Zielhuis and van der Hilst, 1996; Simons et al., 1999]. This concept of constructing a synthetic array from subarrays deployed at different times will probably be applied in the huge-scale USarray project described in section 4.3.

[94] This discussion of temporary arrays is incomplete and highly biased because of our incomplete knowledge of all experiments. For more information on other temporary arrays the reader is referred to the large instrument pools, for example, to the IRIS/PASSCAL Incorporation Research Institutions for Seismology (IRIS)/Program for Array Seismic Studies of the Continental Lithosphere [Vernon et al., 1997] and the German GeoForschungsZentrum section 2.2 web page (<http://www.gfz-potsdam.de/pb2/pb22/projects/projects.html>) for old and recent seismic array experiments.

#### 4.3. Networks

[95] In the 1960s the development of the World-Wide Standardized Seismograph Network (WWSSN) led to new insights into Earth's structure, plate tectonics, and earthquake sources, as well as improvement in locating earthquakes. A total of 140 globally distributed stations with similar instruments provide a homogeneous database and have started a renaissance of seismological research. The stations of the WWSSN were either short-period or long-period stations. Unfortunately, it turned out that by filtering out the medium periods by using either long- or short-period instruments, important information in the seismic signal was also suppressed.

[96] A more recent approach to establish a global broadband seismic network is the Global Seismographic Network (GSN), a part of the IRIS consortium, which has greatly improved our understanding of the Earth. The goal of this network is to deploy  $\sim 130$  permanent seismic recording stations (broadband seismometers) uniformly over the Earth [Butler et al., 2000]. As of 2001, the GSN consisted of over 120 stations, and 13 new stations were planned for 2001/2002. The stations are affiliated with many national and international networks (e.g., IRIS U.S. Geological Survey USGS, IRIS International Deployment of Accelerometers, GeoForschungsNetz, Pacific21, New China Digital Seismographic Network, Advanced Research Projects Agency, and Bundesanstalt für Geowissenschaften und Rohstoffe). In the context of global networks we have to mention the Federation of Digital Broad-Band Seismograph Networks (FDSN), a global organization of groups that operate more than one broadband station either within

their geographical boundaries or globally. FDSN coordinates station siting, station equipment, and data formats and provides open access to their data.

[97] In the early 1990s an extension to the existing Gräfenberg array was planned and set up beginning in November 1991. This network, the German Regional Seismic Network, now consists of 15 seismographic stations distributed all over Germany (approximately  $8^\circ \times 4^\circ$ ). Each station is equipped with a three-component broadband sensor (STS-2 [Wielandt and Steim, 1986]), and the interstation spacing is  $\sim 200$  km.

[98] In the United States several networks have been deployed, for example, the Southern California Seismic Network (SCSN), the Northern California Seismic Network, TriNet (in southern California), and the Pacific Northwest Seismic Network. The SCSN is the largest and most automated network worldwide and consists of more than 350 digital and analog seismometers distributed across southern California. It is also part of TriNet which is jointly operated by the United States Geological Survey, California Institute of Technology, and the California Division of Mines and Geology. For more information on regional networks in the United States and globally, see the information at IRIS (<http://www.iris.washington.edu/>).

[99] An interesting approach is followed for Japanese networks. The so-called J-array is not an array in the narrower sense [J-array Group, 1993]; it combines 14 regional networks run by different universities and institutions. It has a total of 160 seismic stations spread over 2000 km along the Japanese island arc [Morita, 1996]. Because the array was not uniformly built and the regional seismic networks are operated independently, the waveforms from different networks cannot be easily compared. Nonetheless, waveforms can be obtained from one central data center. An attempt to unify the J-array has been started by building the “New-J-Array” [Morita, 1996].

[100] The most recent project for a large array/network is the plan of the USArray. If accomplished, this project will consist of three components (as of 2002, funding is not yet secured). The first component of USArray, similar in approach to SKIPPY, is a transportable telemetered array of 400 broadband seismometers. The transportable array will roll across the United States with 18- to 24-month deployments at each site in configurations providing a station spacing of  $\sim 70$  km and an aperture of  $\sim 1400$  km. The array will record local, regional, and teleseismic earthquakes, providing resolution of crustal and upper mantle structure on the order of tens of kilometers and increased resolution of structures in the lower mantle and of the core-mantle boundary. The second component of USArray is an additional pool of  $\sim 2400$  instruments (200 broadband, 200 short-period, and 2000 high-frequency) that can be deployed using flexible source-receiver geometries. These additional portable instruments will allow for high-density, shorter-term observations of key targets within the footprint of the larger transportable array using both natural

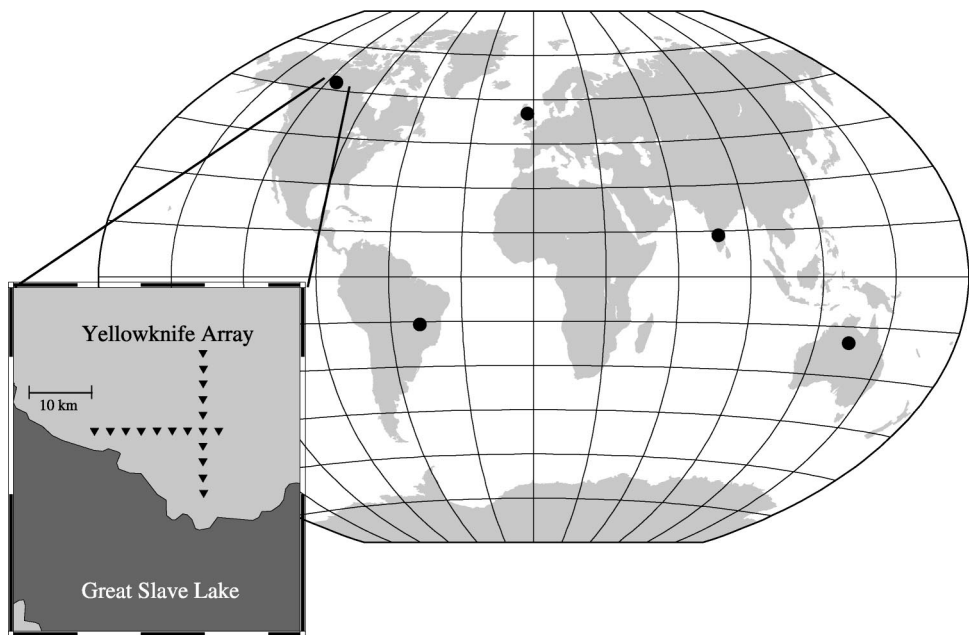


**Figure 21.** Location of the U.K. Atomic Energy Administration type of array. The arrays are EKA (Eskdalemuir, Scotland), GBA (Gauribidanur, India), WRA (Warramunga, Australia), BDF (Brasilia), and YKA (Yellowknife, Canada). The inset shows the configuration of the Canadian Yellowknife array.

and active sources. A third element of USArray is an augmentation of the National Seismic Network, operated by the U.S. Geological Survey. Relatively dense, high-quality observations from a continental network with uniform spacing of 300–350 km are important for tomographic imaging of deep Earth structure, providing a platform for continuous long-term observations, and establishing fixed reference points for calibration of the transportable array [Levander *et al.*, 1999; Meltzer *et al.*, 1999; Iris Consortium, 1999]. Following this policy, USArray will provide excellent data to study the structure of the crust and the upper mantle beneath the United States.

#### 4.3.1. Small Arrays

[101] The first arrays built after the start of negotiations on a comprehensive ban on underground nuclear testing in the late 1950s were rather small, compared to the huge detection arrays built in the 1970s. Several countries, notably the United Kingdom and the United States, were pioneers in the design of arrays capable of detection of nuclear explosions in the teleseismic distance range of 3000–10,000 km. The United Kingdom's nuclear monitoring program led to the construction of an array at Pole Mountain (Wyoming, United States) in 1961, which was dismantled in August 1968 because of severe noise problems [Birtill and Whiteway, 1965]. The successors of this array were the U.K. small-aperture arrays (also called UKAEA arrays, because of their funding by the U.K. Atomic Energy Administration) deployed on five continents: North America (Canada), South America (Brazil), Europe (Scotland), Asia (India), and Australia. These arrays are still operative today (Figure 21). A detailed description of these arrays is

given by, for example, Keen *et al.* [1965]. The UKAEA-type arrays have apertures of ~20 km (except Eskdalemuir (Scotland), which has an aperture of ~8 km) and are equipped with around 20 stations. The configuration is cross- or L-shaped. The configuration of YKA is shown in the inset of Figure 21. The spacing of the stations is 2–3 km. The configurations vary slightly, because of the local geology. Owing to their cross- or L-shaped configuration these arrays have different resolutions in different azimuths, as shown in the fk diagram in Figure 13. The distance between the array stations is the reason for the sidelobes (Figure 13). The size of the arrays and the interstation spacing of these arrays makes them most suitable for *P* wave studies in the 1-Hz range. Despite these shortcomings these arrays have helped to reduce the detection threshold of nuclear explosions and are still used in recent studies [e.g., Bostock and Sacchi, 1997; Rost and Weber, 2001].

#### 4.3.2. Mini Arrays

[102] The first seismological arrays built in the late 1950s and the early 1960s were very small circular arrays with apertures of just a few kilometers (e.g., Blue Mountain array, Uinto Basin array, Tonto Forest array, and Cumberland Plateau array [Romney, 1985]) built within the Vela Uniform Program (United States). The arrays were built with 10–36 seismometers on concentric rings with maximum radii of 2–10 km. The sites were selected with special emphasis on a low noise level and high signal sensitivity of the stations. Because the stations were operated with analog recording, real-time operation was impossible [Husebye and Ruud, 1989]. These arrays were operational for ~10 years.

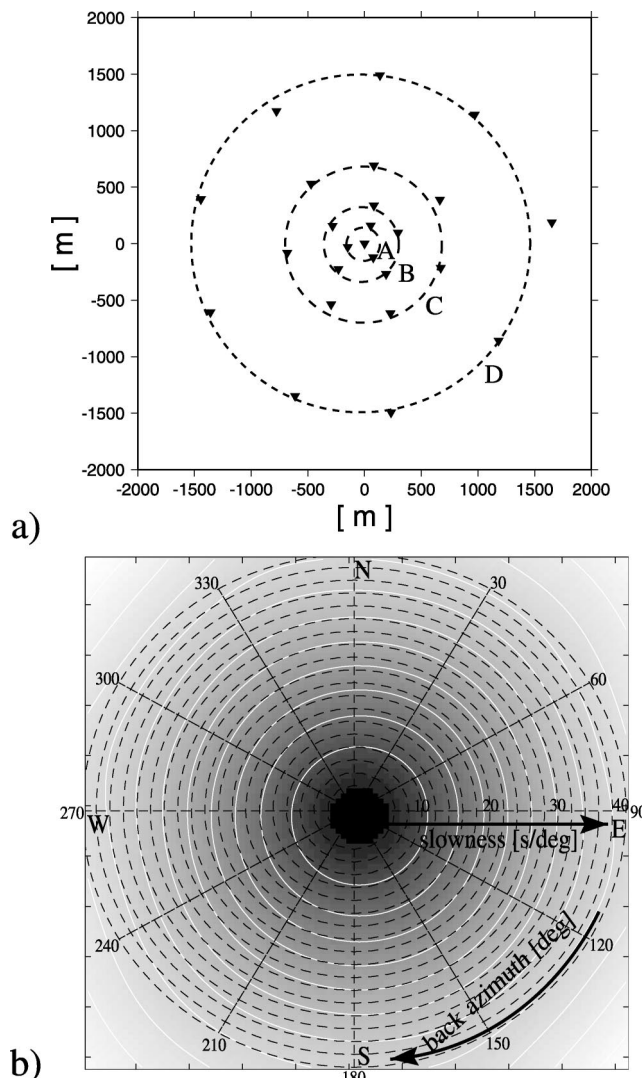


**Figure 22.** (a) Configuration of German Experimental Seismic System (GERESS). The vertical short-period seismometers are arranged on concentric rings with a maximum radius of  $\sim 2$  km. The data are sent via fiber optic cable to the control center near the reference station at the midpoint. One station per ring is equipped with a three-component short-period instrument. (b) Array response function of the 25-element GERESS array (Germany). The power is displayed logarithmically with the sharp maximum (0 dB) at a slowness of 0 s $^{-1}$ . The white lines show  $-1$ -dB isolines. The black lines show the slowness and azimuth grid with the back azimuth and slownesses from 0 s $/deg$  to 40 s $/deg$ . The array response function shows a  $\delta$ -peak-like structure and no azimuthal directivity.

[103] Arrays of this type were built again in the 1980s for nuclear monitoring. Modern arrays of this class are the Norwegian Experimental Seismic System (NORESS) type of array, for example, ARCESS (Norway), Finnish Experimental Seismic System (Finland), German Experimental Seismic System (GERESS) (Germany), and NORESS (Norway).

[104] The configuration of the German GERESS array is shown in Figure 22a. The 25 seismometers are located on concentric rings around a central station. The

maximum diameter of the outermost ring is  $\sim 2$  km. The stations are generally equipped with vertical short-period seismometers, while one instrument per ring is a short-period three-component seismometer (except the outermost D ring, which has two three-component instruments). The configuration of the seismometers on concentric circles with irregular station spacing results in a sharp maximum of the array response function [Haubrich, 1968]. The NORESS-like design of GERESS is aimed to detect weak coherent signals, but owing to the small aperture of the arrays the event location capability is poor [Harris, 1982; Ruud *et al.*, 1988], although because of the setup, the ARF does not show any azimuthal directivity (Figure 22b).

#### 4.4. Suggestions for New Arrays

[105] In the future many new arrays will be deployed, either temporarily or permanently, because of the many advantages seismological arrays offer. After working with data from different arrays, we would like to offer some suggestions on how to configure new arrays. Of course, the planning of a new array depends on available funding, the number of stations, the geology of the subsurface, and the focus of the study for which the array is built. However we have to keep in mind that even if an array is built for only one purpose, we may want to use its data later for studying other regions as well. As discussed in section 4.2.2, linear arrays are very useful for waves that travel along strike across the array. In this case the slowness resolution is very good, but the back azimuth resolution will be restricted. Linear arrays are easy to set up and easy to maintain, but they can only focus on a very restricted source region. Conversely, arrays like NORSAR or LASA have an array transfer-function which closely resembles a delta peak, with high resolution and a minimum of ambiguity. Obviously, an array of this size can hardly be realized nowadays. The small arrays (e.g., GERESS or ARCESS) use a similar station setup, with fewer stations. Because of their small aperture the slowness resolution is restricted.

[106] In our opinion, arrays should have a two-dimensional structure, for example, the cross-shaped structures of the small arrays like YKA, ESK, or WRA, to give a good array transfer function. The arrays, consisting of two lines, show a strong azimuthal dependence of the resolution and are therefore not ideal. Triangle- or rectangle-shaped arrays show a similar azimuthal dependence with sidelobes very close to the main lobe [Harjes and Henger, 1973].

[107] A good compromise is the combination of a circular array with two or more straight lines as suggested by Haubrich [1968]. These arrays with irregular station spacing show a distinctive maximum of the ARF with small sidelobes and no azimuthal dependence of the ARF. The final array configuration is highly dependent on the noise conditions at the array. Dependent on the noise correlation and the signal studied, the array setup can be optimized [Mykkeltveit *et al.*, 1983].

[108] Another important point to bear in mind when constructing an array is the aperture and interstation spacing of the array. These parameters depend on the phases that will typically be studied. To be able to study *P* waves, the interstation spacing should be smaller than 10–20 km to account for the higher frequency of teleseismic *P*. For *S* waves, larger distances between stations are more appropriate (50–100 km). To guarantee coherency of waves across the array, the aperture of the array has to be limited for *P* waves to <100 to 200 km and for *S* waves to less than a few degrees.

## 5. DISCUSSION AND CONCLUSIONS

[109] In this review article we have presented an overview of the most common and some older analysis tools applied to array data. We have discussed different array types and showed the advantages and disadvantages of methods and array configurations.

[110] Array seismology has greatly stimulated the study of the Earth's interior. The advantages of two-dimensional wave field sampling as provided by seismological arrays are obvious. All arrays discussed here are deployments on continents. The deployment of stations solely on shore leaves large “white” spots on the fine-scale seismological map of the Earth's interior. Deployments of seismological arrays on the ocean floor are a new development in this branch of seismology and may help in the more detailed study of many features in the Earth's interior [Laske *et al.*, 1999; Butler *et al.*, 2000].

[111] Owing to technical developments the storage of large amounts of data is less a problem nowadays than some years ago, but efforts must be undertaken to secure older array records like the LASA data set and to transfer the data to modern media [Hedlin *et al.*, 2000]. Several arrays store data based on a triggering mechanism to ensure the storage of “relevant” data. Mostly, only very short time windows are stored, which is especially problematic for studies that use phases arriving later in the wave field [e.g., Castle and van der Hilst, 2000]. A continuous recording of the data stream for all arrays deployed globally is highly desirable. To enable easier access to recorded data, the data must be accessible via the Internet with common retrieval tools like automatic data request manager (autodrm) [Kradolfer, 1993].

[112] Arrays were very beneficial for global seismology in the past. Although they cannot solve all outstanding questions in global seismology, the deployment of more permanent and temporary arrays worldwide, especially in the Southern Hemisphere, is desirable; it will answer some of the open questions and perhaps raise many more.

[113] **ACKNOWLEDGMENTS.** We thank Art Jonkers, Frank Krüger, and two anonymous reviewers for helpful com-

ments and Mike Hedlin for his LASA and NORSAR figure. Maps were produced using GMT [Wessel and Smith, 1991]. The data processing was performed using the Seismic Handler Code by K. Stammiller. C. Thomas was supported by DFG grant TH763/1-1. S. Rost is supported by NSF grant EAR-9905733 (NSF CSEDI).

Louise Kellogg was the Editor responsible for this paper. She thanks one anonymous cross-disciplinary reviewer and two anonymous technical reviewers.

## REFERENCES

- Achauer, U., and the KRISP Working Group, New ideas on the Kenya rift based on the inversion of the combined dataset of the 1985 and 1989/90 seismic tomography experiments, *Tectonophysics*, 236, 305–329, 1994.
- Aki, K., and P. G. Richards, *Quantitative Seismology, Theory and Methods*, vols. I and II, W. H. Freeman, New York, 1980.
- Al-Eqabi, G. I., M. E. Wysession, P. J. Shore, K. M. Fischer, and T. J. Clarke, Upper mantle structure under the north-eastern United States from the inversion of regional and teleseismic Rayleigh waves recorded by the MOMA array (abstract), *Seismol. Res. Lett.*, 67, 29, 1996.
- Arlitt, R., E. Kissling, J. Ansorge, and TOR Working Group, 3-D crustal structure beneath the TOR array and effects on teleseismic wavefronts, *Tectonophysics*, 314, 309–319, 1999.
- Bear, L. K., G. L. Pavlis, and G. H. R. Bokelmann, Multi-wavelet analysis of three-component seismic arrays: Application to measure effective anisotropy at Piñon Flats, California, *Bull. Seismol. Soc. Am.*, 89, 693–705, 1999.
- Berteussen, K. A., The origin of slowness and azimuth anomalies at large arrays, *Bull. Seismol. Soc. Am.*, 66, 719–741, 1976.
- Bilek, S. L., and T. Lay, Lower mantle heterogeneity beneath Eurasia imaged by parametric migration of shear waves, *Phys. Earth Planet. Inter.*, 108, 201–218, 1998.
- Birtill, J. W., and F. E. Whiteway, The application of phased arrays to the analysis of seismic body waves, *Philos. Trans. R. Soc. London, Ser. A*, 258, 421–493, 1965.
- Bostock, M. G., and S. Rondenay, Migration of scattered teleseismic body waves, *Geophys. J. Int.*, 137, 732–746, 1999.
- Bostock, M. G., and M. D. Sacchi, Deconvolution of teleseismic recordings for mantle structure, *Geophys. J. Int.*, 129, 143–152, 1997.
- Bracewell, R. N., The Fourier transform and its applications, McGraw-Hill, New York, 1965.
- Butler, R., et al., Hawaii-2 Observatory pioneers opportunities for remote instrumentation in ocean studies, *Eos Trans. AGU*, 81, 151, 162–163, 2000.
- Buttkus, B., Ten years of the Gräfenberg array, *Geol. Jahrb. Reihe E*, 35, 135 pp., 1986.
- Capon, J., Signal processing and frequency-wavenumber spectrum analysis for a large aperture seismic array, *Methods Comput. Phys.*, 13, 1–59, 1973.
- Castle, J. C., and K. C. Creager, A steeply dipping discontinuity in the lower mantle beneath Izu-Bonin, *J. Geophys. Res.*, 104, 7279–7292, 1999.
- Castle, J. C., and R. D. van der Hilst, The core-mantle boundary under the Gulf of Alaska: No ULVZ for shear waves, *Earth Planet. Sci. Lett.*, 176, 311–321, 2000.
- Cotte, N., H. A. Pedersen, M. Campillo, V. Farra, and Y. Cansi, Of great-circle propagation of intermediate-period surface waves observed on a dense array in the French alps, *Geophys. J. Int.*, 142, 825–840, 2000.
- Dainty, A. M., Studies of coda using array and three-component processing, *Pure Appl. Geophys.*, 132, 221–244, 1990.

- Davies, D., E. J. Kelly, and J. R. Filson, Vespa process for analysis of seismic signals, *Nature Phys. Sci.*, 232, 8–13, 1971.
- Doornbos, D. J., and E. S. Husebye, Array analysis of PKP phases and their precursors, *Phys. Earth Planet. Inter.*, 6, 387–399, 1972.
- Douglas, A., Making the most of the recordings from short-period seismometer arrays, *Bull. Seismol. Soc. Am.*, 88, 1155–1170, 1998.
- Douglas, A., Seismometer arrays—Their use in earthquake and test ban seismology, in *Handbook of Earthquake and Engineering Seismology*, edited by P. Jennings, H. Kanamori, and W. Lee, 357–367, Academic, San Diego, Calif., 2002.
- Douglas, A., D. Bowers, P. D. Marshall, J. B. Young, D. Porter, and N. J. Wallis, Putting nuclear-test monitoring to the test, *Nature*, 398, 474–475, 1999.
- Earle, P. S., Origins of high-frequency scattered waves near PKKP from large aperture seismic array data, *Bull. Seismol. Soc. Am.*, 92, 751–760, 2002.
- Frosch, R. A., and P. E. Green, The concept of the large aperture seismic array, *Proc. R. Soc. London, Ser. A*, 290, 368–384, 1966.
- Goldstein, P., W. R. Walter, and G. Zandt, Upper mantle structure beneath central Eurasia using a source array of nuclear explosions and waveforms at regional distances, *J. Geophys. Res.*, 97, 14,097–14,115, 1992.
- Gregersen, S., et al., Important findings expected from Europe's largest seismic array, *Eos Trans. AGU*, 80, 1, 6, 1999.
- Haddon, R. A. W., E. S. Husebye, and D. W. King, Origins of precursors to P'P', *Phys. Earth Planet. Inter.*, 14, 41–70, 1977.
- Harjes, H.-P., and M. Henger, Array-Seismologie, *Z. Geophys.*, 39, 865–905, 1973.
- Harris, D. B., Uncertainty in direction estimation: A comparison of small arrays and three-component stations, *Tech. Rep. UCID-19589*, Lawrence Livermore Nat. Lab., Livermore, Calif., 1982.
- Hastings, D. A., and P. K. Dunbar, Development and assessment of the global land one-km base elevation digital elevation model (GLOBE), *ISPRS Arch.*, 32, 218–221, 1998.
- Haubrich, R. A., Array design, *Bull. Seismol. Soc. Am.*, 58, 977–991, 1968.
- Haykin, S. (Ed.), *Array Signal Processing*, Prentice-Hall, Englewood Cliffs, N. J., 1985.
- Hedlin, M. A. H., J. B. Minster, and J. A. Orcutt, Beam stack imaging using a small aperture array, *Geophys. Res. Lett.*, 18, 1771–1774, 1991.
- Hedlin, M. A. H., P. Earle, and H. Bolton, Old seismic data yield new insights, *Eos Trans. AGU*, 81, 469, 472–473, 2000.
- Helffrich, G., S. Kaneshima, and J.-M. Kendall, A local, crossing-path study of attenuation and anisotropy of the inner core, *Geophys. Res. Lett.*, 29, 1568, doi:10.1029/2001GL014059 2002.
- Husebye, E. S., and D. W. King, Precursors to PKIKP and seismic wave scattering near the core-mantle boundary, *J. Geophys. Res.*, 81, 1870–1882, 1976.
- Husebye, E. S., and B. O. Ruud, Array seismology—Past, present and future developments, in *Observatory Seismology*, edited by J. J. Litehiser, pp. 123–153, Univ. of Calif. Press, Berkeley, 1989.
- Husebye, E. S., A. Dahle, and K.-A. Berteussen, Bias analysis of NORSAR- and ISC-reported seismic event  $m_b$  magnitudes, *J. Geophys. Res.*, 79, 2967–2978, 1974.
- Hwang, L. J., and R. W. Clayton, A station catalog of ISC arrivals: Seismic station histories and station residuals, *U.S. Geol. Surv. Open File Rep.*, 91–295, 1991.
- Ingate, S. F., E. S. Husebye, and A. Christofferson, Regional arrays and optimum data processing schemes, *Bull. Seismol. Soc. Am.*, 75, 1155–1177, 1985.
- IRIS Consortium, USArray—A component of Earthscope, report, Earth Sci. Div., Nat. Sci. Found., Arlington, Va., 1999.
- J-array Group, The J-array program: System and present status, *J. Geomagn. Geoelectr.*, 45, 1265–1271, 1993.
- Jahnke, G., Analyse schwacher telesismischer Einsätze an kleinen Arrays: Möglichkeiten und Grenzen, *Diplomarbeit, Georg-August Univ. Göttingen*, Germany, 1998.
- Jurkevics, A., Polarization analysis of three-component array data, *Bull. Seismol. Soc. Am.*, 78, 1725–1743, 1988.
- Kanasewich, E. R., *Time Sequence Analysis in Geophysics*, Univ. of Alberta Press, Alberta, Vict., Canada, 1981.
- Kanasewich, E. R., C. D. Hemmings, and T. Alpaslan, Nth-root stack nonlinear multichannel filter, *Geophysics*, 38, 327–338, 1973a.
- Kanasewich, E. R., R. M. Ellis, C. H. Chapman, and P. R. Gutowski, Seismic array evidence of a core boundary source for the Hawaiian linear volcanic chain, *J. Geophys. Res.*, 78, 1361–1371, 1973b.
- Káráson, H., and R. D. van der Hilst, Tomographic imaging of the lowermost mantle with differential times of refracted and diffracted core phases (PKP,  $P_{\text{diff}}$ ), *J. Geophys. Res.*, 106, 6569–6587, 2001.
- Kay, I., S. Sol, J.-M. Kendall, C. J. Thomson, D. White, I. Asudeh, B. Roberts, and D. Francis, Shear wave splitting observations in the Archean craton of Western Superior, *Geophys. Res. Lett.*, 26, 2669–2672, 1999.
- Keen, C. G., J. Montgomery, W. M. H. Mowat, and D. C. Platt, British seismometer array recording systems, *Radio Electron. Eng.*, 30, 297–306, 1965.
- Kelly, E. J., Response of seismic signals to wide-band signals, *Lincoln Lab. Tech. Note 1967 30*, Lincoln Lab., Mass. Inst. of Technol., Lexington, Mass., 1967.
- Kennett, B. L. N., and E. R. Engdahl, Traveltimes for global earthquake location and phase identification, *Geophys. J. Int.*, 105, 429–465, 1991.
- Kennett, B. L. N., and R. D. van der Hilst, Using a synthetic continental array to study the Earth's interior, *J. Phys. Earth*, 44, 669–674, 1996.
- King, D. W., R. A. W. Haddon, and E. S. Husebye, Precursors to PP, *Phys. Earth Planet. Inter.*, 10, 103–127, 1975.
- King, D. W., E. S. Husebye, and R. A. W. Haddon, Processing of seismic precursor data, *Phys. Earth Planet. Inter.*, 12, 128–134, 1976.
- Koper, K. D., T. C. Wallace, S. R. Taylor, and H. E. Hartse, Forensic seismology and the sinking of the Kursk, *Eos Trans. AGU*, 82, 37, 45–46, 2001.
- Kradolfer, U., Automating the exchange of earthquake information, *Eos Trans. AGU*, 74, 442, 444–445, 1993.
- Krüger, F., and M. Weber, The effect of low velocity sediments on the mislocation vectors of the GRF array, *Geophys. J. Int.*, 108, 387–393, 1992.
- Krüger, F., M. Weber, F. Scherbaum, and J. Schlittenhardt, Double beam analysis of anomalies in the core-mantle boundary region, *Geophys. Res. Lett.*, 20, 1475–1478, 1993.
- Krüger, F., F. Scherbaum, M. Weber, and J. Schlittenhardt, Analysis of asymmetric multipathing with a generalisation of the double-beam method, *Bull. Seismol. Soc. Am.*, 86, 737–749, 1996.
- Krüger, F., M. Baumann, F. Scherbaum, and M. Weber, Mid mantle scatterers near the Mariana slab detected with a double array method, *Geophys. Res. Lett.*, 28, 667–670, 2001.
- Kuwahara, Y., H. Ito, H. Kawakatsu, T. Ohminato, and T. Kiguchi, Crustal heterogeneity as inferred from seismic coda wave decomposition by small-aperture array observation, *Phys. Earth Planet. Inter.*, 104, 247–256, 1997.
- Kværna, T., On exploitation of small-aperture NORESS type arrays for enhanced P-wave detectability, *Bull. Seismol. Soc. Am.*, 79, 888–900, 1989.

- Kværna, T., and D. J. Doornbos, An integrated approach to slowness analysis with arrays and three-component stations, *Rep. NORSAR 2-85/86*, Norw. Seismic Array, Kjeller, Norway, 1986.
- Laske, G., J. Phipps Morgan, and J. A. Orcutt, First results from the Hawaiian SWELL Pilot Experiment, *Geophys. Res. Lett.*, 26, 3397–3400, 1999.
- Lay, T., Analysis of near source contributions to early  $P$ -wave coda for underground explosions, III, Inversion for isotropic scatterers, *Bull. Seismol. Soc. Am.*, 77, 1767–1783, 1987.
- Lay, T., and C. S. Lynnes, Inversion of  $P$  coda for isotropic scatterers at the Yucca Flat test site, *Bull. Seismol. Soc. Am.*, 79, 790–804, 1989.
- Lay, T., and C. J. Young, Imaging scattering structures in the lower mantle by migration of long-period  $S$  waves, *J. Geophys. Res.*, 101, 20,023–20,040, 1996.
- Levander, A., E. D. Humphreys, G. Ekstrom, A. S. Meltzer, and P. M. Shearer, Proposed project would give unprecedented look under North America, *Eos Trans. AGU*, 80, 245, 250–251, 1999.
- Lynnes, C. S., and T. Lay, Inversion of  $P$  coda for isotropic scatterers at the Yucca Flat test site, *Bull. Seismol. Soc. Am.*, 79, 790–804, 1989.
- McFadden, P. L., B. J. Drummond, and S. Kravis, The  $N$ -th root stack: Theory, applications, and examples, *Geophysics*, 51, 1879–1892, 1986.
- Meltzer, A., et al., USAArray initiative, *GSA Today*, 9, (11), 8–10, 1999.
- Morita, Y., The characteristics of J-array seismograms, *J. Phys. Earth*, 44, 657–668, 1996.
- Muirhead, K. J., and R. Datt, The  $N$ -th root process applied to seismic array data, *Geophys. J. R. Astron. Soc.*, 47, 197–210, 1976.
- Mykkeltveit, S., K. Astebol, D. J. Doornbos, and E. S. Husebye, Seismic array configuration optimization, *Bull. Seismol. Soc. Am.*, 73, 173–186, 1983.
- Neal, S. L., and G. L. Pavlis, Imaging  $P$ - to  $S$  conversions with multichannel receiver functions, *Geophys. Res. Lett.*, 26, 2581–2584, 1999.
- Neal, S. L., and G. L. Pavlis, Imaging  $P$ - to  $S$  conversions with broad-band seismic arrays using multichannel time-domain deconvolution, *Geophys. J. Int.*, 146, 57–67, 2001.
- Neidell, N. S., and M. T. Taner, Semblance and other coherency measures for multichannel data, *Geophysics*, 36, 482–497, 1971.
- Niazi, M., Use of source arrays in studies of regional studies, *Bull. Seismol. Soc. Am.*, 59, 1631–1643, 1969.
- Oldenburg, D. W., A comprehensive solution to the linear deconvolution problem, *Geophys. J. R. Astron. Soc.*, 65, 331–357, 1981.
- Pavlis, G. L., and H. Mahdi, Surface wave propagation in central Asia: Observations of scattering and multipathing with the Kyrgyzstan broadband array, *J. Geophys. Res.*, 101, 8437–8455, 1996.
- Posmentier, E. S., and R. W. Herrmann, Cophase: An ad hoc array processor, *J. Geophys. Res.*, 76, 2194–2201, 1971.
- Revenaugh, J., The contribution of topographic scattering to teleseismic coda in southern California, *Geophys. Res. Lett.*, 22, 543–546, 1995.
- Ritter, J. R. R., U. R. Christensen, U. Achauer, K. Bahr, and M. Weber, Search for a mantle plume under central Europe, *Eos Trans. AGU*, 79, 420, 1998.
- Ritter, J. R. R., M. Jordan, U. Christensen, and U. Achauer, A mantle plume below the Eifel volcanic fields, Germany, *Earth Planet. Sci. Lett.*, 186, 7–14, 2001.
- Romney, C. F., VELA Overview: The early years of seismic research program, in *The VELA Program: Twenty-Five Years of Basic Research*, edited by A. U. Kerr, pp. 38–65, Def. Adv. Res. Proj. Agency, Rosslyn, Va., 1985.
- Rost, S., and J. Revenaugh, Seismic detection of rigid zones at the top of the core, *Science*, 294, 1911–1914, 2001.
- Rost, S., and M. Weber, A reflector at 200 km depth beneath the NW Pacific, *Geophys. J. Int.*, 147, 12–28, 2001.
- Rothert, E., and J. R. R. Ritter, Small-scale heterogeneities below the Gräfenberg array, Germany, from seismic wavefield fluctuations of Hindu Kush events, *Geophys. J. Int.*, 140, 175–184, 2001.
- Ruud, B. O., E. S. Husebye, S. F. Ingate, and A. Christoffersen, Event location at any distance using seismic data from a single, three-component station, *Bull. Seismol. Soc. Am.*, 78, 308–325, 1988.
- Scherbaum, F., D. Gillard, and N. Deichmann, Slowness power spectrum analysis of the coda composition of two micro-earthquake clusters in northern Switzerland, *Phys. Earth Planet. Inter.*, 67, 137–161, 1991.
- Scherbaum, F., F. Krüger, and M. Weber, Double beam imaging: Mapping lower mantle heterogeneities using combinations of source and receiver arrays, *J. Geophys. Res.*, 102, 507–522, 1997.
- Schimmel, M., and H. Paulsen, Noise reduction and detection of weak, coherent signals through phase weighted stacks, *Geophys. J. Int.*, 130, 497–505, 1997.
- Simons, F. J., A. Zielhuis, and R. D. Van der Hilst, The deep structure of the Australian continent inferred from surface wave tomography, *Lithos*, (48/1-4), 17–43, 1999.
- Spudich, P., and T. Bostwick, Studies of the seismic coda using an earthquake cluster as a deeply buried seismograph array, *J. Geophys. Res.*, 92, 10,526–10,546, 1987.
- Thomas, C., M. Weber, C. Wicks, and F. Scherbaum, Small scatterers in the lower mantle observed at German broadband arrays, *J. Geophys. Res.*, 104, 15,073–15,088, 1999.
- Thomas, C., J.-M. Kendall, and M. Weber, Images of  $D'$  beneath northern Asia, I, Multi-azimuth studies of heterogeneity, in press, *Geophys. J. Int.*, 2002.
- Tolstoy, I., H. Montes, G. Rao, and E. Willis, Long period sound waves in the thermosphere from Apollo launches, *J. Geophys. Res.*, 75, 5621–5625, 1970.
- van der Hilst, R. D., B. Kennett, D. Christie, and J. Grant, Project Skippy explores the mantle and lithosphere beneath Australia, *Eos Trans. AGU*, 75, 177, 180–181, 1994.
- Vernon, F., D. Quinlan, G. L. Pavlis, G. Offield, D. Harvey, M. Glushko, and K. Dueker, The first deployment of the IRIS PASSCAL broadband array, *Eos Trans. AGU*, 78, Fall Meet. Suppl. F462, 1997.
- Vidale, J. E., and P. S. Earle, Fine-scale heterogeneity in the Earth's inner core, *Nature*, 404, 273–275, 2000.
- Vidale, J. E., D. A. Dodge, and P. S. Earle, Slow differential rotation of the Earth's inner core indicated by temporal changes in scattering, *Nature*, 405, 445–448, 2000.
- Wagner, G. S., Regional wave propagation in southern California and Nevada: Observations from a three-component seismic array, *J. Geophys. Res.*, 102, 8285–8311, 1997.
- Wagner, G. S., and T. J. Owens, Broadband bearing-time records of three-component seismic array data and their application to the study of local earthquake coda, *Geophys. Res. Lett.*, 20, 1823–1826, 1993.
- Weber, M. H.,  $P$ - and  $S$ -wave reflections from anomalies in the lowermost mantle, *Geophys. J. Int.*, 115, 183–210, 1993.
- Weber, M., and C. W. Wicks Jr., Reflections from a distant subduction zone, *Geophys. Res. Lett.*, 23, 1453–1456, 1996.
- Weber, M., J. P. Davis, C. Thomas, F. Krüger, F. Scherbaum, J. Schlittenhardt, and M. Körnig, The structure of the lowermost mantle as determined from using seismic arrays, in *Seismic Modeling of the Earth's Structure*, edited by E. Boschi, G. Ekström, and A. Morelli, pp. 399–442, Institut Naz. di Geophys., Rome, 1996.
- Weichert, D. H., Reduced false alarm rates in seismic array

- detection by non-linear beam-forming, *Geophys. Res. Lett.*, 2, 121–123, 1975.
- Wessel, P., and W. H. F. Smith, Free software helps map and display data, *Eos Trans. AGU*, 72, 441, 445–446, 1991.
- Whiteway, F. E., The use of arrays for earthquake seismology, *Proc. R. Soc. London, Ser. A*, 290, 328–342, 1966.
- Wielandt, E., and J. M. Stein, A digital very-broad-band seismograph, *Ann. Geophys. Ser. B*, 4, 227–232, 1986.
- Wielandt, E., and G. Streckeisen, The leaf-spring seismometer: Design and performance, *Bull. Seismol. Soc. Am.*, 72, 2349–2367, 1982.
- Wright, C., Array studies of seismic waves arriving between  $P$  and  $PP$  in the distance range  $90^\circ$  to  $115^\circ$ , *Bull. Seismol. Soc. Am.*, 62, 385–400, 1972.
- Wysession, M. E., Large-scale structure of the core-mantle boundary from core-diffracted waves, *Nature*, 382, 244–248, 1996.
- Wysession, M. E., K. M. Fischer, T. J. Clarke, G. I. Al-eqabi, M. J. Fouch, L. A. Salvati, P. J. Shore, and R. W. Valenzuela, Slicing into the Earth: Seismic mapping with the Missouri-to-Massachusetts broadband deployment, *Eos Trans. AGU*, 77, 480–482, 1996.
- Wysession, M. E., A. Langenhorst, M. J. Fouch, G. I. Al-eqabi, P. J. Shore, and T. J. Clarke, Lateral variations in compressional/shear velocities at the base of the mantle, *Science*, 284, 120–125, 1999.
- Yilmaz, Ö., *Seismic Data Processing*, Soc. of Explor. Geophys., Tulsa, Okla., 1987.
- Ying, J., and H.-C. Nataf, Detection of mantle plumes in the lower mantle by diffraction tomography: Hawaii, *Earth Planet. Sci. Lett.*, 159, 99–115, 1998.
- Zielhuis, A., and R. D. van der Hilst, Upper-mantle shear velocity beneath eastern Australia from inversion of waveforms from SKIPPY portable arrays, *Geophys. J. Int.*, 127, 1–16, 1996.

---

S. Rost, Department of Earth Sciences, IGPP-CSIDE, University of California Santa Cruz, 1156 High Street, Santa Cruz, CA 95064, USA. (srost@es.ussc.edu)

C. Thomas, Department of Earth Sciences, University of Liverpool, 4 Downlow Street, Liverpool, L69 3GP, UK. (tine@liv.ac.uk)